Part III
Cardiology

Chapter 12
Noninvasive PET Flow Reserve Imaging to Direct Optimal Therapies for Myocardial Ischemia

Robert A. deKemp and Rob SB Beanlands

Abstract Nuclear cardiology imaging with SPECT or PET is used widely in North America for the diagnosis and management of patients with coronary artery disease. Conventional myocardial perfusion imaging (MPI) can identify areas of reversible ischemia as suitable targets for coronary artery revascularization by angioplasty or bypass surgery. However, the accuracy of this technique is limited in patients with advanced disease in multiple coronary arteries, where there is no normal reference territory against which to assess the "relative" perfusion defects. We have developed methods for the routine quantification of absolute myocardial blood flow (MBF mL/min/g) and coronary flow reserve (stress/rest MBF) using rubidium-82 dynamic PET imaging. The incremental diagnostic and prognostic value of absolute flow quantification over conventional MPI has been demonstrated in several recent studies. Clinical use of this added information for patient management to direct optimal therapy and the potential to improve cardiac outcomes remains unclear, but may be informed by recent progress and widespread clinical adoption of invasive fractional flow reserve(FFR)-directed revascularization. This paper presents recent progress in this field, toward noninvasive CFR image-guided therapy with cardiac PET and SPECT.

Keywords Noninvasive cardiac imaging • Myocardial ischemia • Myocardial blood flow • Coronary flow reserve • Positron emission tomography

12.1 Introduction

Improvements in diagnostic imaging and therapeutic methods have helped to reduce the cardiac death rate in Canada and other developed nations over the past decade [16]. However, cardiovascular disease is still the number one cause of death in most industrialized countries [3]. Noninvasive diagnostic imaging is used

R.A. deKemp (✉) • R.S. Beanlands
National Cardiac PET Centre, Division of Cardiology, University of Ottawa Heart Institute, Ottawa, ON, Canada
e-mail: radekemp@ottawaheart.ca

Y. Kuge et al. (eds.), *Perspectives on Nuclear Medicine for Molecular Diagnosis and Integrated Therapy*, DOI 10.1007/978-4-431-55894-1_12

increasingly as a "gatekeeper" to help optimize the most effective use of higher-risk invasive (and costly) diagnostic and interventional procedures, such as coronary angiography and revascularization.

This work is motivated in part by the recent FAME trials [7, 38] showing that impaired flow reserve, when used to identify "flow-limiting" epicardial stenoses for revascularization, improved clinical outcomes (reduced cardiac death and myocardial infarction rates) and lowered the total cost of treatment. The FAME trials used *invasive angiography* measurements of fractional flow reserve (FFR), but with associated risks of embolic stroke and other complications of coronary artery catheterization that may be avoided with the use of *noninvasive imaging* methods.

Myocardial perfusion reserve (MPR) imaging using positron emission tomography (PET) may enable diagnosis of patients with microvascular disease (uVD) or nonobstructive diffuse epicardial disease, who should *not* be recommended for coronary revascularization, sparing them the unnecessary risks of invasive angiography for diagnosis alone. Some enhancements to the conventional methods of PET flow reserve imaging are proposed for accurate noninvasive imaging of *ischemia*, to improve identification of hemodynamically and physiologically significant "flow-limiting" lesions that are optimal targets for invasive revascularization. According to recent AHA/NIH publications [28], "Standard tests used to diagnose CAD are not designed to detect coronary uVD. More research is needed to find the best diagnostic tests and treatments for the disease." The flow reserve concepts used in this study are illustrated in Fig. 12.1, and the specific terms are defined in Table 12.1.

Current international practice guidelines [1, 2] recommend the use of treadmill exercise-ECG testing and stress perfusion imaging for the diagnosis of ischemia (benefit class I, evidence levels A,B) and the use of invasive flow reserve (FFR) measurements to direct invasive revascularization (benefit class I, IIa, evidence level A) for the treatment of symptoms in patients with suspected ischemic heart disease. Despite a wealth of observational data, stress MPI is still not a class 1 (A) indication to direct revascularization in patients with stable ischemic heart

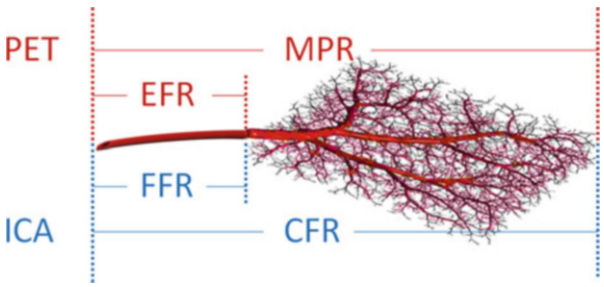

Fig. 12.1 Epicardial (EFR, FFR) ± microvascular (MPR, CFR) flow reserve measurements using PET imaging and ICA. Normal values of MPR and CFR are approximately 3–5 (average 4.0) in young healthy adults without microvascular disease. Normal epicardial vessels have FFR = 1.0, whereas "flow-limiting" stenoses with FFR < 0.75–0.80 can produce myocardial ischemia. See Table 12.1 for definitions

Table 12.1 Flow reserve terminology

Name	Definition
Coronary artery disease (CAD)	Focal or diffuse narrowing of an *epicardial* coronary artery lumen due to the formation of atherosclerotic plaque (stenosis or lesion) in the arterial wall
Microvascular disease (uVD)	Damage to the inner lining (endothelium) of the *subepicardial* small arteries or arterioles that regulate blood flow to the heart muscle
Myocardial blood flow (MBF)	*Microvascular* perfusion [mL/min/g] of blood to the heart muscle
Myocardial perfusion (flow) reserve (MPR, MFR)	**Ratio** of maximal hyperemic stress/rest perfusion (tissue flow), including the effects of *epicardial and microvascular* disease, typically measured using noninvasive PET imaging (Fig. 12.1)
Microvascular reserve (uVR)	**Ratio** of endothelium-dependent stress/rest MBF in the small resistance arteries and arterioles
Epicardial flow reserve (EFR)	**Ratio** of epicardial vessel-dependent stress/rest MBF in the large conduit arteries. The sum total of uVR + EFR is equal to MPR
Coronary flow reserve (CFR)	**Ratio** of maximal hyperemic stress/rest blood flow in the epicardial coronary arteries, reflecting the effects of *epicardial and microvascular* disease. CFR is typically measured invasively during adenosine stress using the indicator dilution technique
Fractional flow reserve (FFR)	**Fraction** of pressure maintained across an *epicardial* stenosis during hyperemic stress, measured using invasive angiography. It is analogous to the relative MPR value, in single-vessel disease without uVD

disease because there remains insufficient evidence that ischemia-directed therapy reduces the risk of death and/or myocardial infarction.

In conjunction with, or following exercise-ECG testing, stress myocardial perfusion imaging (MPI) is used widely in North America for the noninvasive diagnosis of coronary artery disease. While single-photon emission computed tomography (SPECT) is used most commonly, rubidium-82 (^{82}Rb) PET has been available in the USA since 1989 for the diagnosis of obstructive coronary artery disease (CAD). We recently completed enrolment of >15,000 patients in the Canadian multicenter trial [8] evaluating ^{82}Rb PET as an alternative radiopharmaceutical for myocardial perfusion imaging (Rb-ARMI). Initial results confirmed the high accuracy (>90 %) of low-dose ^{82}Rb PET-CT for diagnosis of obstructive coronary artery disease in patients with epicardial stenoses ≥ 50–70 % [20]. Recent meta-analyses also confirm that PET has higher accuracy for diagnosis of CAD compared to SPECT, even when using current cameras with attenuation correction and ECG-gating [24].

Stress perfusion imaging is also used for the assessment of myocardial ischemia, to identify patients that will benefit from invasive revascularization therapy procedures such as coronary angioplasty and bypass surgery [15] as shown in Fig. 12.2. The efficacy of this approach was suggested initially in the nuclear sub-study of the

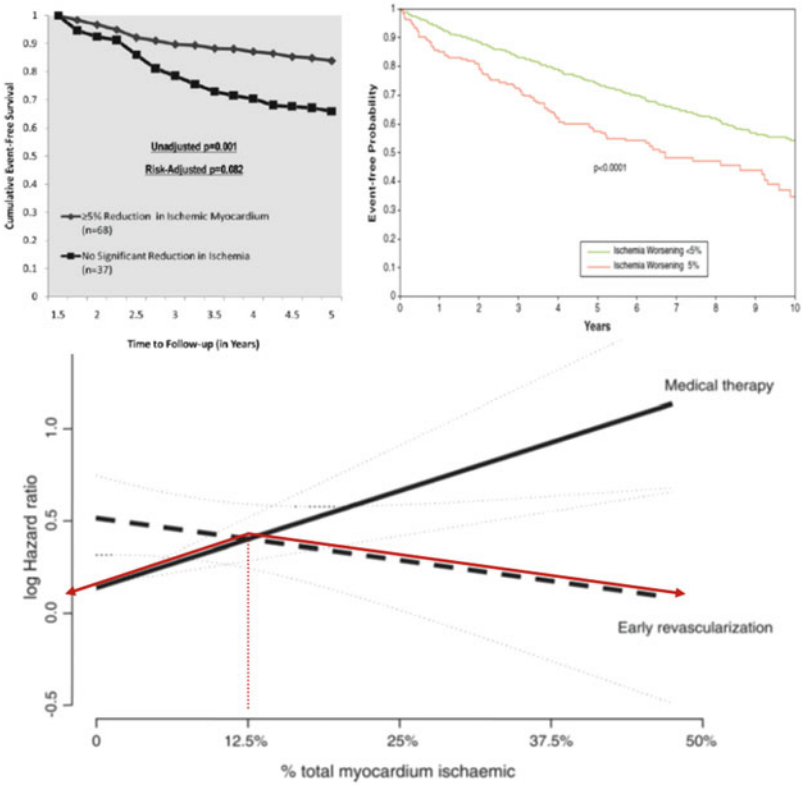

Fig. 12.2 Patients with moderate-to-severe ischemia in the COURAGE nuclear sub-study (A) had a lower rate of death or MI when there was a 5 % improvement (reduction) in ischemic burden following revascularization. In the DUKE nuclear cardiology registry (B), patients with >5 % ischemia worsening had increased risk of death or MI. Retrospective analysis of ~14,000 SPECT-MPI patients (C) indicated that the percent ischemic myocardium (>10–15 %) predicted lower risk (log hazard ratio) of death following early revascularization. In patients with less than 10–15 % ischemic myocardium, medical therapy was the most effective treatment [Reproduced from (A) [37], (B) [12], and (C) [15].]

COURAGE trial [37] and confirmed recently in patients from the DUKE registry [12], showing survival and outcome benefits from invasive revascularization using angioplasty in addition to optimal medical (drug) therapy, in patients with at least *5 % ischemic myocardium* improvement. The ISCHEMIA trial currently in progress [23] is intended to verify prospectively, in patients with ischemia by physiological testing (for MPI: at least 10 % ischemic left ventricular (LV) myocardium), whether or not revascularization compared to medical therapy will result in improved clinical outcomes. This is a pivotal trial intended to prove conclusively the value of ischemia detection by stress perfusion imaging. However, but it is important to recognize that conventional stress MPI (using SPECT or PET) will still underestimate the extent and severity of ischemia from diffuse or multivessel

disease (patients with left-main coronary artery disease are excluded) and will neither identify - nor direct treatment of - high-risk patients with disease of the coronary microvasculature.

12.2 Myocardial Blood Flow (Perfusion) Imaging

Some limitations of conventional (relative) MPI can be overcome by quantifying myocardial perfusion blood flow (MBF) in absolute units of mL/min/g. Dynamic imaging is required starting from the time of tracer injection, to capture the first-pass transit through the venous-arterial circulation as shown in Fig. 12.3. The concentration of tracer is measured over time in the arterial blood and myocardial tissues, and the rate of uptake or transfer from blood to tissue (influx rate K1 mL/min/g) is related to the absolute myocardial perfusion [21]. Flow quantification restores the true normal-to-diseased tissue contrast (Fig. 12.4), which is otherwise underestimated by measurement of the tracer retention (net uptake) alone. It also allows visualization of the stress/rest perfusion or flow reserve (MPR or MFR) as a measure of the total coronary vascular dilator capacity.

A one-tissue-compartment model is often used to describe the early kinetics (e.g., 0–5 min) of tracer exchange between the arterial blood supply and myocardial target tissues. This model has been validated for rubidium-82 (^{82}Rb) imaging in humans using nitrogen-13 (^{13}N)-ammonia PET as the reference standard [22] and

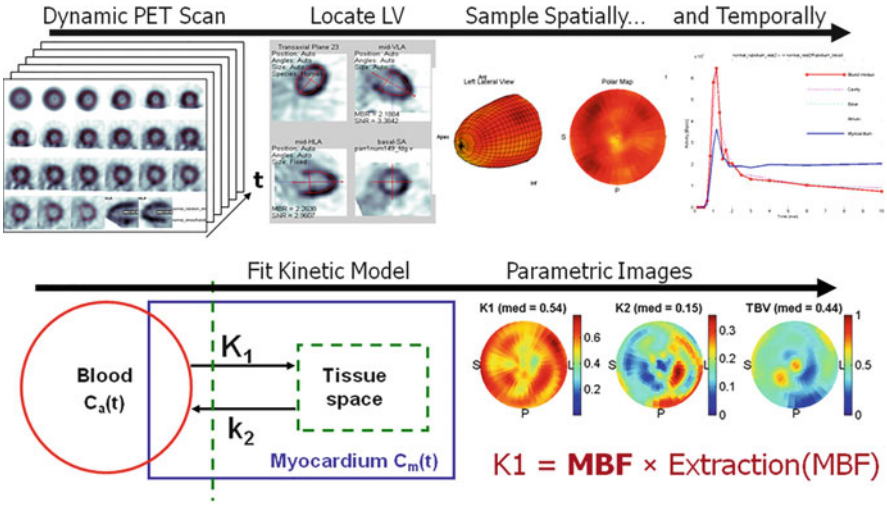

Fig. 12.3 Quantification of MBF using dynamic PET imaging. Dynamic images are acquired starting at the time of tracer injection, then activity in the LV cavity and myocardium is measured over time and fit to a one-tissue-compartment model of the tracer kinetics. The influx rate of tracer uptake or transfer from blood to tissue (K1 mL/min/g) is related to MBF, according to a tracer extraction function E(MBF)

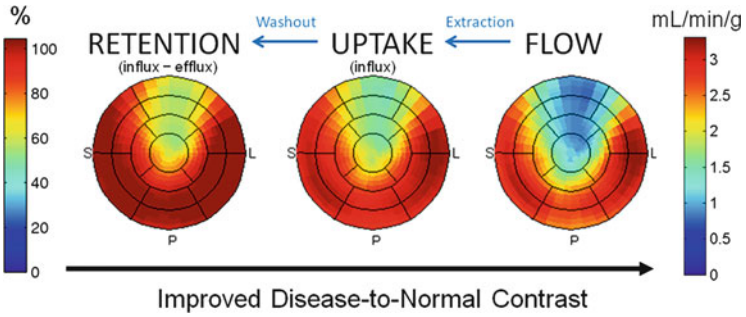

Fig. 12.4 Polar-maps of MBF (flow), ^{82}Rb uptake (K1 influx rate), and retention (net influx – efflux) demonstrating the effects of nonlinear tracer extraction and washout. MBF estimation restores the true disease-to-normal tissue contrast and increases the sensitivity to detect focal disease relative to areas of maximal flow

has been demonstrated to give very reproducible results using several investigational and commercial implementations as shown in Fig. 12.5a, b [9, 27, 31]. Test-retest repeatability of the method (Fig. 12.5c) is approximately 10–12 % CV (coefficient of variation) at rest and 6–7 % during pharmacologic stress [11, 30], comparable to the theoretical expected values verified recently using Monte-Carlo and analytic simulations [25].

Resting MBF is known to correlate highly with the metabolic demands of normal cardiac work [4] as shown in Fig. 12.6; therefore, it is common to adjust the rest of the MBF values to an average reference standard value (e.g., 8500 in typical patients). There a normal age-related increase in RPP, which also contributes to a progressive decline in MPR [10]. The adjusted values at rest represent the expected MBF under conditions of normal controlled systolic blood pressure and heart rate, which are often elevated in patients undergoing stress MPI. The RPP-adjusted MPR represents the flow reserve that would be expected in a patient with normal resting hemodynamics, which may be used to evaluate impairments in coronary vasodilator function associated with atherosclerosis that are unbiased by the effects of resting hypertension.

Because of the wide physiological variability in rest MBF values between patients, interpretation of absolute PET flow studies is recommended to include *both* the stress MBF *and* the stress/rest perfusion reserve in combination [18] as illustrated in Fig. 12.7. Abnormalities in both flow reserve < 1.5–2 and stress MBF < 1 mL/min/g have been suggested to represent ischemic tissues that should be considered for revascularization [17]. The absolute flow increase (stress–rest MBF delta) has also been proposed as an alternative method to evaluate the vasodilator response in some studies of vascular endothelial function [36] but has not been as widely applied in practice.

The diagnostic utility of PET MPR assessment has been confirmed in patients with multivessel disease [40]. As shown in Fig. 12.8a, there is a 50 % likelihood of three-vessel disease in patients with a global LV flow reserve that is severely

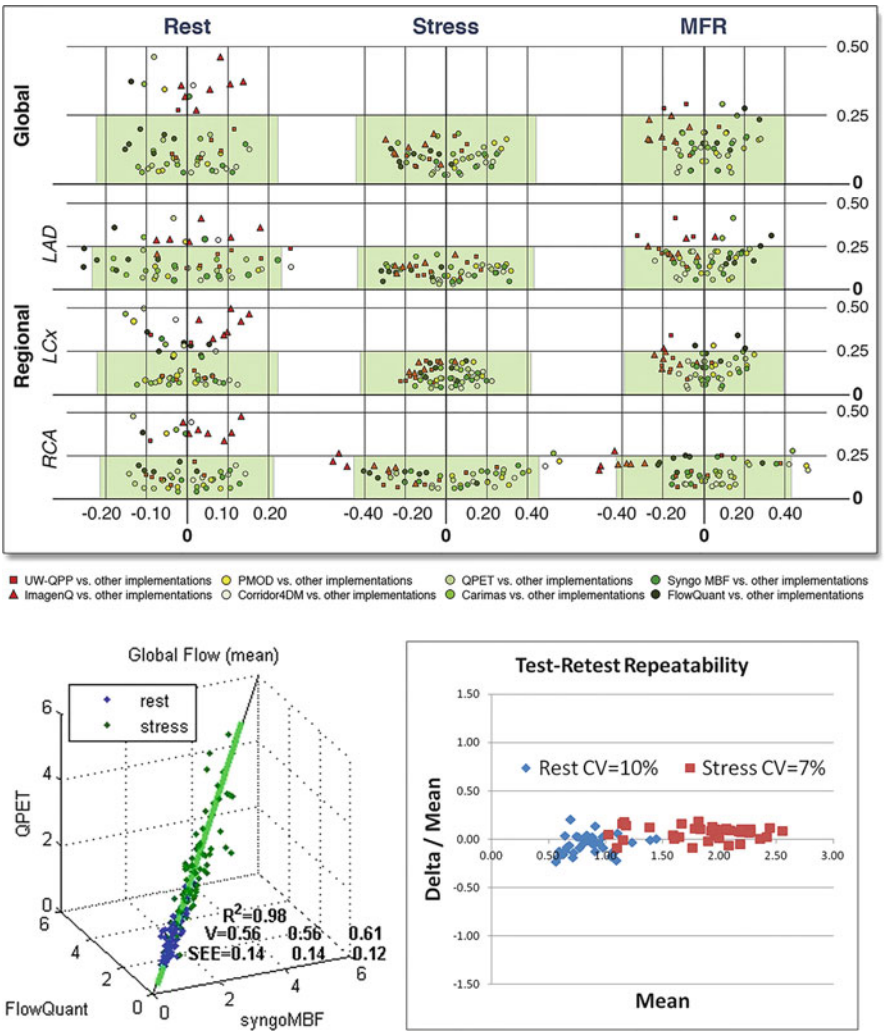

Fig. 12.5 MBF values measured using the one-tissue-compartment model are highly reproducible between several investigational (A) and commercial (B) software implementations. Rest and stress flow values are generally within 15–20 %, allowing multicenter data to be pooled or combined between vendors. Test–retest repeatability is 7–10 % at stress and rest (C), for single-session back-to-back scans

impaired (MPR = 1), whereas the balance of patients presumably have severe microvascular disease limiting their ability to increase myocardial perfusion from rest to peak stress. Measurements of absolute MPR also have prognostic value that is incremental and independent of the standard assessments of relative MPI [41], as shown in Fig. 12.8b. Patients with normal MPI (SSS < 4) but abnormal flow reserve (MFR < 2) are at increased risk of cardiac events. In the case of abnormal MPI, if

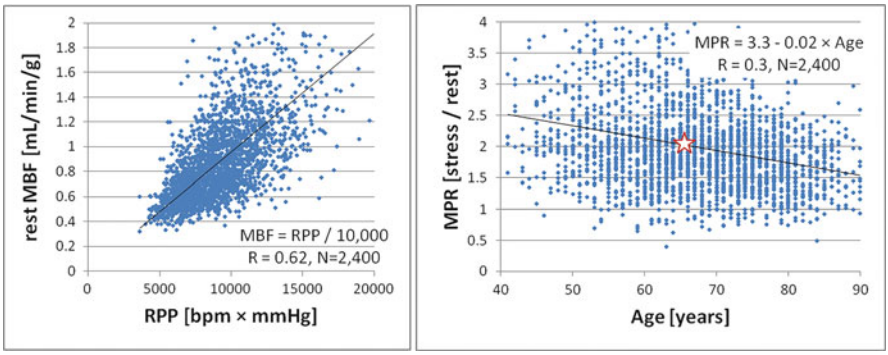

Fig. 12.6 MBF at rest is correlated with the heart rate × systolic blood pressure product (RPP). Peak stress/rest MPR decreases with age as a result of changes in microvascular reactivity and diffuse atherosclerosis. A median MPR value of 2.0 is observed at age 65 (red star)

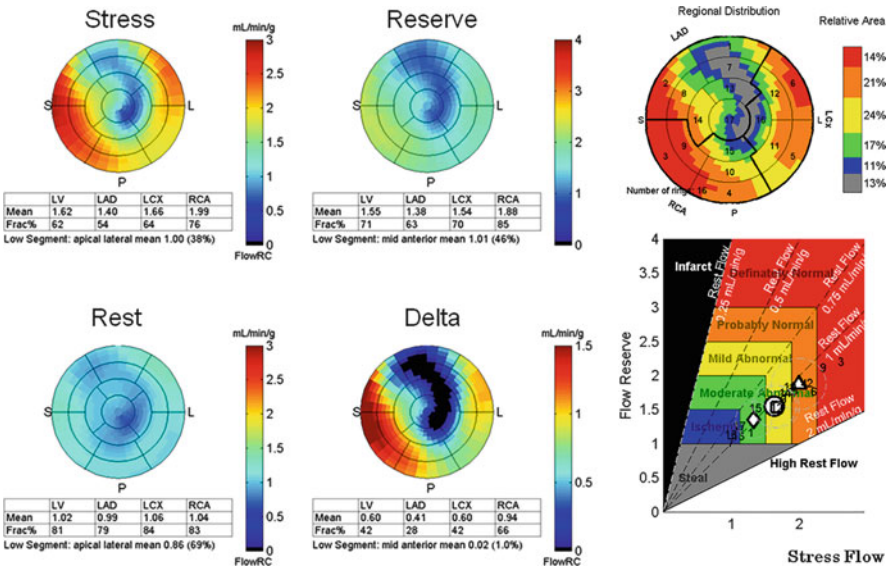

Fig. 12.7 Clinical interpretation of PET quantitative MBF measurements at rest, stress, stress/rest reserve (MPR), and stress–rest delta. The "regional distribution" map is a combination of the flow reserve and stress flow maps, according to the scheme shown on the bottom right

flow reserve is also impaired, then these patients have the highest rate of cardiac events within the following year. Similar findings have reported in a separate cohort of ischemic heart disease patients [26]; those with the lowest values of MPR had the highest cardiac event rates. Despite these observational studies, there is a lack of evidence proving that revascularization of ischemic myocardium as identified by absolute flow imaging will result in a lower risk of cardiac death or myocardial infarction.

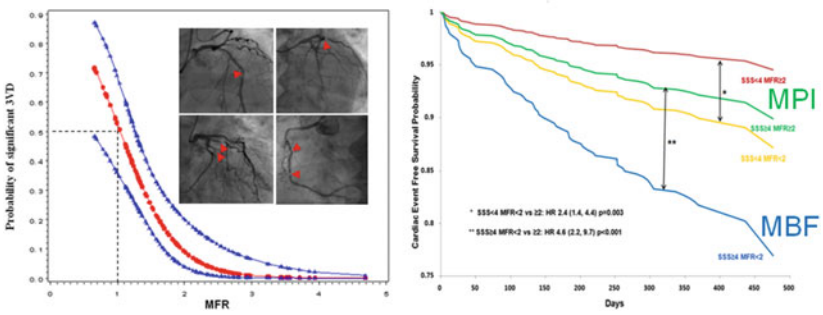

Fig. 12.8 Diagnostic utility of MPR (MFR) in multivessel disease is shown on the left [40]. Patients with global flow reserve < 1 have > 50 % probability of three-vessel disease; the remaining patients have severe microvascular disease. Patients with reductions in flow reserve (MFR < 2) have lower event-free survival, regardless of whether their relative perfusion (SSS) is normal or abnormal [41]

12.3 Fractional Flow Reserve Assessment

Invasive coronary angiography methods have been developed over the past two decades to quantify the functional or hemodynamic significance of epicardial coronary artery disease, using proximal-distal pressure measurements of the fractional flow reserve ratio (FFR) [13], as illustrated in Fig. 12.9. FFR is defined as the fractional pressure drop measured across one or more stenoses in an individual coronary artery. Interestingly, invasive measurements of FFR were originally validated against ^{15}O-water PET measurements of *relative* MPR [5]. As shown in Fig. 12.10, coronary FFR values were similar to the relative MPR on average, whereas the myocardial FFR shows a small bias of approximately +10 % vs. the PET analogous values.

Epicardial stenoses with abnormal FFR < 0.75 were initially shown to identify the presence of myocardial ischemia with high accuracy compared to a positive test on one or more of three noninvasive methods: exercise thallium planar imaging, *or* dobutamine stress echocardiography, *or* treadmill exercise ECG (Fig. 12.11) [33, 34]. This FFR threshold is therefore very sensitive for the detection of ischemia, because it correlates with ischemia on *any* of the reference standards above.

Test-retest repeatability of FFR measurements has been reported in the range of 4–7 % CV [6, 29, 32], similar to the precision of PET stress MBF (Fig. 12.12). This has led to the adoption of a 5 % "gray zone" of uncertainty in FFR measurements considered to be hemodynamically significant or flow limiting.

The pivotal FAME trial [38] showed that percutaneous coronary intervention (PCI) revascularization using coronary stenting of anatomically *and* hemodynamically significant lesions (stenosis ≥ 50 % *and* FFR ≤ 0.80) improved cardiac outcomes (Fig. 12.13) and reduced the total cost of treatment compared to the standard practice of revascularization for anatomically significant lesions only

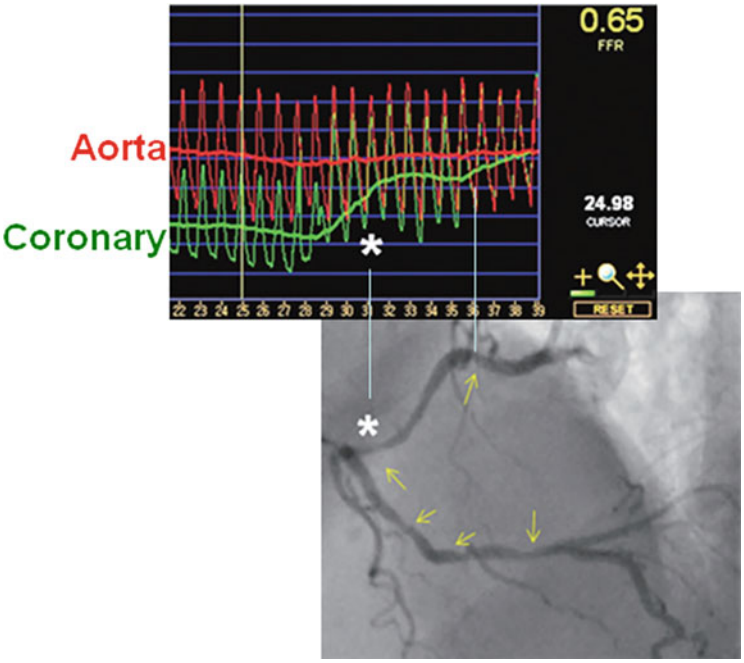

Fig. 12.9 Fractional flow reserve is measured as the ratio of intracoronary pressure distal to a stenosis and relative to the (proximal normal) aortic pressure during peak adenosine pharmacologic stress. Comparison of the FFR measurements to coronary angiography allows identification of flow-limiting stenoses that are optimal targets for revascularization

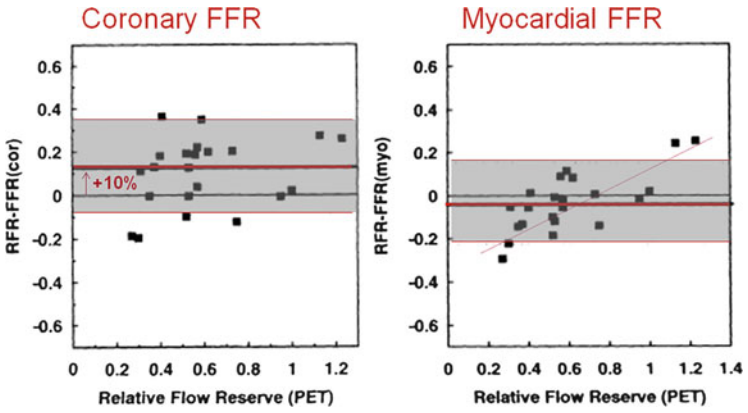

Fig. 12.10 Invasive measurements of FFR were originally validated against ^{15}O-water PET MBF studies in a group of N = 22 patients with single-vessel coronary artery disease. Coronary (epicardial) FFR produced values that were ~10 % higher than the relative flow reserve (relative MPR) values. The myocardial (epicardial + microvascular) FFR values corrected for atrial venous pressure were more accurate on average, but demonstrated an increasing trend versus PET. Adapted from [5]

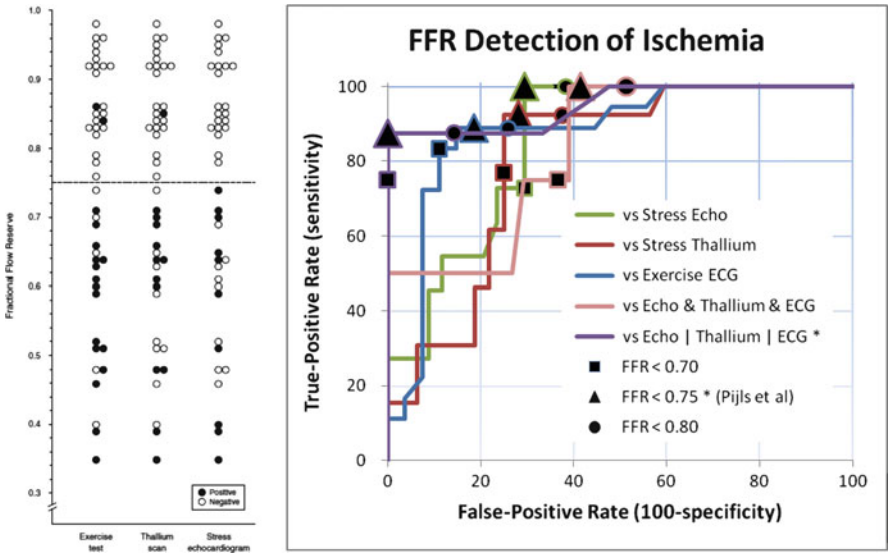

Fig. 12.11 Fractional flow reserve (FFR) compared to ischemia testing in N = 45 patients, using exercise ECG, thallium imaging, and stress echo [34]. Abnormal FFR < 0.75 was reported to have 88 % sensitivity and 100 % specificity to identify ischemia according to stress echo or exercise thallium imaging or exercise-ECG tests combined(*), but specificity decreases dramatically in the "gray zone" between the FFR cutoff values of 0.75 to 0.80 and when FFR is compared individually to the ischemia standard tests. At the FFR cutoff value < 0.80 commonly used to direct revascularization, fewer than 50 % of subjects had exercise-ECG, stress echo, and thallium tests that were all positive for ischemia

(stenosis > 50–70 %). However, there remains a significant cost (interventional pressure wires) and patient morbidity (risk of embolic strokes) associated with this invasive procedure. While FFR provides a useful physiological assessment of epicardial stenoses, it does not assess the severity of microvascular disease and actually underestimates the functional significance of epicardial lesions in the presence of microvascular disease [35]. Despite these limitations, FFR has recently been upgraded to a class I(A) indication in Europe and class IIa(A) in North America for use in directing revascularization therapy to improve clinical outcomes.

12.4 Noninvasive PET (MPR) vs. Invasive Coronary Angiography (FFR)

Reductions in the supply of blood to the myocardium are caused by two separate consequences of disease: (1) epicardial coronary stenoses and (2) microvascular dysfunction. The "flow-limiting" epicardial stenoses should be identified ideally

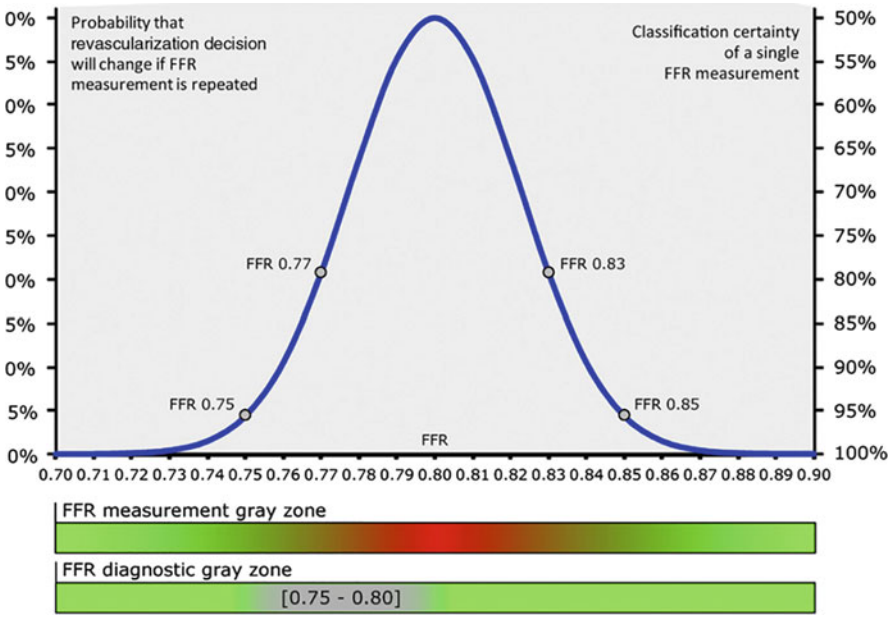

Fig. 12.12 Test-retest repeatability of back-to-back FFR measurements 10 min apart (4 % CV), reanalyzed from the DEFER study by [32]. The measurement (or classification) uncertainty is shown as the red-green colorbar, reflecting the probability that a revascularization decision would change with repeat measurement. The conventional diagnostic uncertainty or "gray zone" of 0.75–0.80 is shown as the grey-green colorbar

as targets for revascularization, whereas patients with diffuse or microvascular disease may be better treated with targeted aggressive medical therapies such as lipid-lowering statins or other novel drug treatments under development to improve endothelial function by increasing nitric-oxide bioavailability, for example.

Myocardial and fractional flow reserve measurements represent different hemodynamic effects of microvascular and epicardial disease. The interrelated physiological interpretation of PET MFR vs. invasive FFR measurements has been the subject of several recent reviews [14, 19]. The discordance between FFR and MPR is attributed to the differences in epicardial vs microvascular disease (Fig. 12.14c) and is consistent with our PET data in over 3,000 patients (Fig. 12.14a, b).

As illustrated in Fig. 12.1, noninvasive PET imaging of MPR measures the capacity to increase perfusion (and tracer delivery) in the downstream microvasculature within the myocardium, reflecting the combined "total" effects of microvascular and epicardial disease. Invasive FFR measures the pressure drop across a

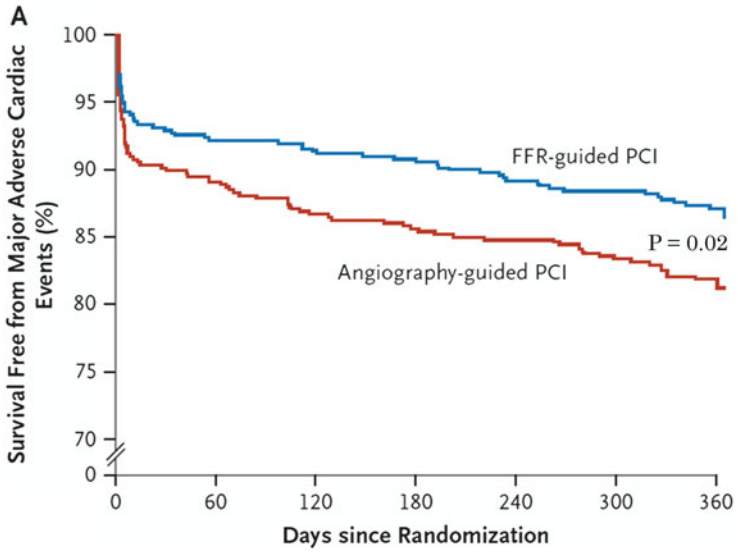

Fig. 12.13 The FAME randomized controlled trial in N = 1005 patients showed that clinical outcome was improved (87 % vs. 82 % event-free survival; p = 0.02) using FFR-guided revascularization by PCI with drug-eluting stents in patients with intermediate-grade stenosis > 50 % and FFR < 0.80. The FFR-guided approach also resulted in 30 % fewer stents placed per patient (p < 0.001) and 11 % lower overall costs including the added FFR pressure wires [38]

single epicardial stenosis during hyperemic stress, representing the peak flow compared to the (restored or expected) normal flow in the absence of stenosis. FFR determines whether a particular epicardial lesion is "flow limiting"; however, this measurement assumes that maximal peak-stress vasodilatation was achieved in the downstream microvasculature. Therefore, *in the presence of microvascular dysfunction*, FFR can be overestimated (i.e., the severity of disease underestimated) due to a submaximal stress flow response, resulting in underdiagnosis and potential undertreatment of the disease [35].

There is a wide variation in reported MFR values at a given lesion stenosis severity (Fig. 12.15a) confirming the influence of confounding variables such as peak-MFR and/or microvascular flow reserve (uVR). Measurements of *total MFR* alone cannot separate the fundamental difference in stress flow responses present in the epicardial conduit arteries vs. the microvascular resistance vessels. This effect is illustrated in Fig. 12.15b showing that a 70 % stenosis can appear to have normal *or* abnormal FFR depending on the peak hyperemic flow response (peak-MFR).

We have proposed a simple model describing MPR as the sum total of uVR and epicardial CFR as shown in Fig. 12.15c. This model is consistent with

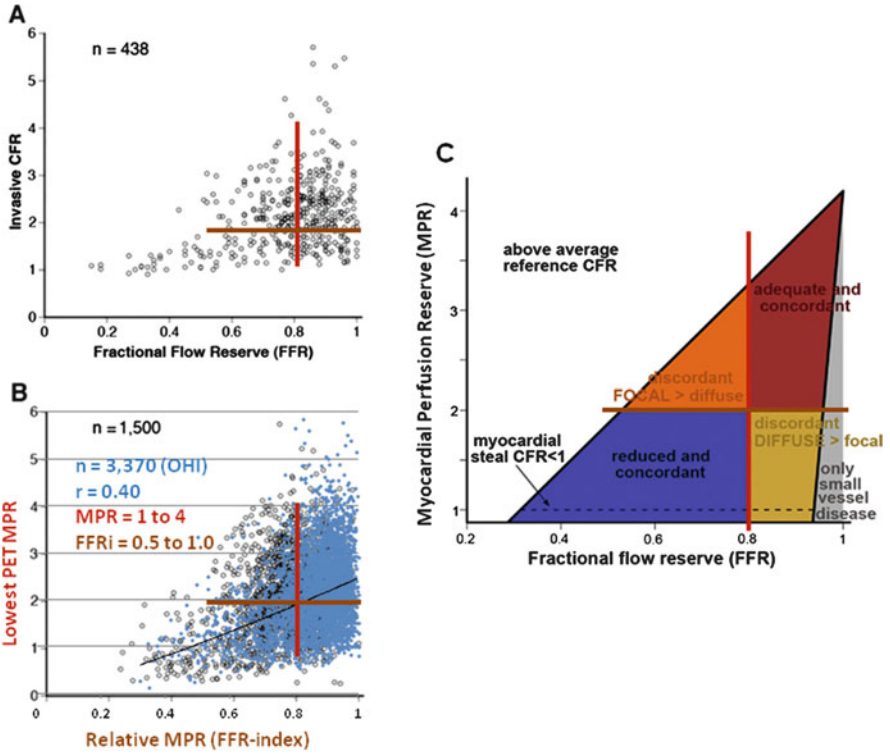

Fig. 12.14 Discordance between FFR and MPR is due to the physiological differences in focal epicardial vs. diffuse or microvascular disease. (A) Invasive [and (B) noninvasive] measures of CFR [and absolute MPR] vs. FFR [and relative MPR] measurements can be discordant in some patients, due to the different physiological consequences of focal vs. diffuse microvascular disease (C). Adapted from [19]

previous observations that MFR decreases with increasing lesion stenosis%, but at different reference levels depending on the burden of microvascular disease. uVR is presumed to be independent of epicardial stenosis severity, also consistent with previous invasive measurements of microcirculatory resistance (IMR) [39]. The model predicts that a particular threshold value (EFR = MPR – uVR) for epicardial coronary revascularization will only improve symptoms of ischemia in patients without severe microvascular disease, e.g., with uVR > 0, as shown in Fig. 12.15d. Conversely, myocardial ischemia may be overestimated in young patients without uVD, where an "apparent ischemic" stress perfusion defect in a patient with very high peak-MFR may still be above the true ischemic threshold of stress MBF.

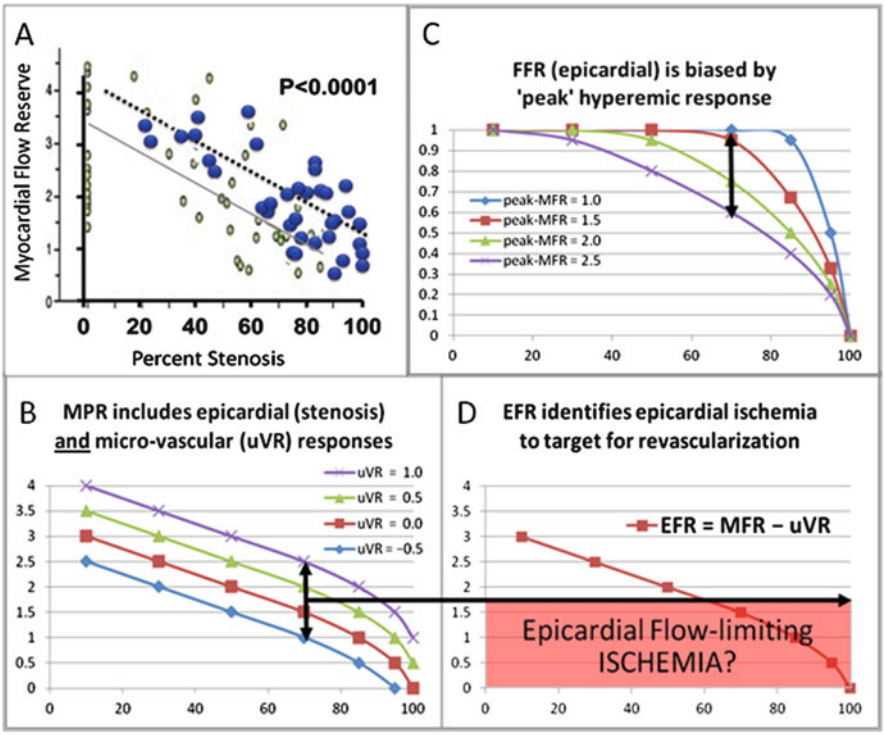

Fig. 12.15 Total myocardial perfusion (flow) reserve (MPR) is a function of epicardial stenosis severity (0–100 %) and microvascular vasodilator response (uVR) as shown in (**A**, **B**). In patients with severe microvascular (endothelial) dysfunction (e.g. uVR = −0.5), invasive measurement of fractional flow reserve (FFR) may appear normal in coronary lesions up to 90 % stenosis (**C**), due to the absence of hyperemic flow response (peak-MFR = 1.0). Epicardial flow reserve (EFR = MPR–uVR) may be useful to identify flow-limiting lesions associated with myocardial ischemia (**D**)

12.5 Conclusion

Noninvasive nuclear imaging of myocardial blood flow (MBF) and coronary flow reserve (CFR) is now feasible as part of the clinical routine using positron emission tomography (PET) imaging. PET measurements of absolute MBF are reliable and reproducible between imaging centers and software methods, with test–retest repeatability below 10 % coefficient of variation. Ischemic thresholds have been proposed for stress MBF and coronary flow reserve in the range of 1.5 [mL/min/g] and 1.0 [stress/rest MBF], respectively. Prospective trials are needed to determine whether patient outcomes can be improved using these ischemic thresholds to direct appropriate revascularization vs. optimal medical therapies.

References

1. ACCF/AHA/SCAI Guideline for Percutaneous Coronary Intervention. J Am Coll Cardiol. 2011;58(24):e44–e122.
2. ACCF/AHA/ACP/AATS/PCNA/SCAI/STS Guideline for the Diagnosis and Management of Patients with Stable Ischemic Heart Disease. J Am Coll Cardiol. 2012;60(24):e44–e164.
3. Canadian Institutes of Health Research *Annual Report* 2010–11. Moving Forward CIHR Performance across the Spectrum: From Research Investments to Knowledge Translation.
4. Czernin J, Porenta G, Brunken R, Krivokapich J, Chen K, Bennett R, Hage A, Fung C, Tillisch J, Phelps ME. Regional blood flow, oxidative metabolism, and glucose utilization in patients with recent myocardial infarction. Circulation. 1993;88(3):884–95.
5. De Bruyne B, Baudhuin T, Melin JA, et al. Coronary flow reserve calculated from pressure measurements in humans. validation with positron emission tomography. Circulation. 1994;89:1013–22.
6. de Bruyne B, Bartunek J, Sys SU, Pijls NH, Heyndrickx GR, Wijns W. Simultaneous coronary pressure and flow velocity measurements in humans. Feasibility, reproducibility, and hemodynamic dependence of coronary flow velocity reserve, hyperemic flow versus pressure slope index, and fractional flow reserve. Circulation. 1996;94(8):1842–9.
7. De Bruyne B, Pijls NH, Kalesan B, Barbato E, Tonino PA, Piroth Z, Jagic N, Möbius-Winkler S, Rioufol G, Witt N, Kala P, MacCarthy P, Engström T, Oldroyd KG, Mavromatis K, Manoharan G, Verlee P, Frobert O, Curzen N, Johnson JB, Jüni P. Fearon WF; FAME 2 Trial Investigators. Fractional flow reserve-guided PCI versus medical therapy in stable coronary disease. N Engl J Med. 2012;367(11):991–1001.
8. deKemp RA, Wells GA, Beanlands RSB. Rubidium-82 – An Alternative Radiopharmaceutical for Myocardial Imaging (Rb-ARMI) 2009–2015. http://clinicaltrials.gov/ct2/show/NCT01128023
9. deKemp RA, DeClerck J, Klein R, Pan X-B, Nakazato R, Tonge C, Arumugam P, Berman DS, Germano G, Beanlands RS, Slomka PJ. Multi-software reproducibility study of stress and rest myocardial blood flow assessed with 3D dynamic PET-CT and a one-tissue-compartment Model of 82Rb Kinetics. J Nucl Med. 2013;54:571–577.
10. deKemp RA, Klein R, Renaud J, Garrard L, Wells GA, Beanlands R. Patient age, gender and hemodynamics are independent predictors of myocardial flow reserve as measured with dipyridamole stress PET perfusion imaging. J Nucl Med. 2014;55(S1):79.
11. Efseaff M, Klein R, Ziadi MC, Beanlands RS, deKemp RA. Short-term repeatability of resting myocardial blood flow measurements using rubidium-82 PET imaging. J Nucl Cardiol. 2012;19(5):997–1006.
12. Farzaneh-Far A, Phillips HR, Shaw LK, Starr AZ, Fiuzat M, O'Connor CM, Sastry A, Shaw LJ, Borges-Neto S. Ischemia change in stable coronary artery disease is an independent predictor of death and myocardial infarction. JACC Cardiovasc Imaging. 2012;5(7):715–24.

13. Gould KL, Kirkeeide RL, Buchi M. Coronary flow reserve as a physiologic measure of stenosis severity. J Am Coll Cardiol. 1990;15(2):459–74.
14. Gould KL. Does coronary flow trump coronary anatomy? JACC Cardiovasc Imaging. 2009;2:1009–23.
15. Hachamovitch R, Rozanski A, Shaw LJ, Stone GW, Thomson LE, Friedman JD, Hayes SW, Cohen I, Germano G, Berman DS. Impact of ischemia and scar on the therapeutic benefit derived from myocardial revascularization vs. medical therapy among patients undergoing stress-rest myocardial perfusion scintigraphy. Eur Heart J. 2011;32(8):1012–24.
16. Heart and Stroke Foundation *Annual report* on Canadians Health. A Perfect Storm of Heart Disease Looming on Our Horizon, January 25, 2010.
17. Johnson NP, Gould KL. Physiological basis for angina and ST-segment change: PET-verified thresholds of quantitative stress myocardial perfusion and coronary flow reserve. JACC Cardiovasc Imaging. 2011;4:990–8.
18. Johnson NP, Gould KL. Integrating noninvasive absolute flow, coronary flow reserve, and ischemic thresholds into a comprehensive map of physiological severity. JACC Cardiovasc Imaging. 2012;5:430–40.
19. Johnson NP, Kirkeeide RL, Gould KL. Is discordance of coronary flow reserve and fractional flow reserve due to methodology or clinically relevant coronary pathophysiology? JACC Cardiovasc Imaging. 2012;5:194–202.
20. Kaster T, Mylonas I, Renaud JM, Wells GA, Beanlands RSB, deKemp RA. Accuracy of low-dose rubidium-82 myocardial perfusion imaging for detection of coronary artery disease using 3D PET and normal database interpretation. J Nucl Cardiol. 2012.
21. Klein R, Renaud JM, Ziadi MC, Beanlands RSB, deKemp RA. Intra- and inter-operator repeatability of myocardial blood flow and myocardial flow reserve measurements using rubidium-82 pet and a highly automated analysis program. J Nucl Cardiol. 2010;17:600–16.
22. Lortie M, Beanlands RS, Yoshinaga K, Klein R, Dasilva JN, deKemp RA. Quantification of myocardial blood flow with 82Rb dynamic PET imaging. Eur J Nucl Med Mol Imaging. 2007;34:1765–74.
23. Maron D, Boden W, Ferguson B, Harrington R, Stone G, Williams D. International study of comparative health effectiveness with medical and invasive approaches (ISCHEMIA). https://clinicaltrials.gov/ct2/show/NCT01471522
24. Mc Ardle BA, Dowsley TF, deKemp RA, Wells GA, Beanlands RS. Does rubidium-82 PET have superior accuracy to SPECT perfusion imaging for the diagnosis of obstructive coronary disease? A systematic review and meta-analysis. J Am Coll Cardiol. 2012;60(18):1828–37.
25. Moody J, Murthy V, Lee B, Corbett J, Ficaro E. Variance Estimation for Myocardial Blood Flow by Dynamic PET. IEEE Trans Med Imaging. 2015 May 13. [Epub ahead of print]
26. Murthy VL, Naya M, Foster CR, Hainer J, Gaber M, Di Carli G, Blankstein R, Dorbala S, Sitek A, Pencina MJ, Di Carli MF. Improved cardiac risk assessment with noninvasive measures of coronary flow reserve. Circulation. 2011;124(20):2215–24.
27. Nesterov SV, Deshayes E, Sciagrà R, Settimo L, Declerck JM, Pan XB, Yoshinaga K, Katoh C, Slomka PJ, Germano G, Han C, Aalto V, Alessio AM, Ficaro EP, Lee BC, Nekolla SG, Gwet KL, deKemp RA, Klein R, Dickson J, Case JA, Bateman T, Prior JO, Knuuti JM. Quantification of myocardial blood flow in absolute terms using (82)Rb PET imaging: the RUBY-10 Study. JACC Cardiovasc Imaging. 2014;7(11):1119–27.
28. NIH-NHLBI website. What is Coronary Microvascular Disease? http://www.nhlbi.nih.gov/health/health-topics/topics/cmd. Accessed September 2015.
29. Ntalianis A, Sels JW, Davidavicius G, Tanaka N, Muller O, Trana C, Barbato E, Hamilos M, Mangiacapra F, Heyndrickx GR, Wijns W, Pijls NH, De Bruyne B. Fractional flow reserve for the assessment of nonculprit coronary artery stenoses in patients with acute myocardial infarction. JACC Cardiovasc Interv. 2010;3(12):1274–81.
30. Ocneanu A, Adler A, Renaud J, Beanlands R, deKemp R, Klein R. Reproducible tracer injection profile improves the test-retest repeatability of myocardial blood flow quantification with 82Rb PET. J Nucl Med. 2015;56(S3):207.

31. Pan X-B, DeClerck J. Validation *syngo* PET Myocardial Blood Flow. Siemens Healthcare: White Paper 2012.
32. Petraco R, Sen S, Nijjer S, Echavarria-Pinto M, Escaned J, Francis DP, Davies JE. Fractional flow reserve-guided revascularization: practical implications of a diagnostic gray zone and measurement variability on clinical decisions. JACC Cardiovasc Interv. 2013;6(3):222–5. doi: 10.1016/j.jcin.2012.10.014. Erratum in: JACC Cardiovasc Interv. 2013;6(4):431.
33. Pijls NH, van Son JA, Kirkeeide RL, De Bruyne B, Gould KL. Experimental basis of determining maximum coronary, myocardial, and collateral blood flow by pressure measurements for assessing functional stenosis severity before and after percutaneous transluminal coronary angioplasty. Circulation. 1993;87:1354–67.
34. Pijls NH, De Bruyne B, Peels K, Van Der Voort PH, Bonnier HJ, Bartunek J, Koolen JJ, Koolen JJ. Measurement of fractional flow reserve to assess the functional severity of coronary-artery stenoses. NEJM. 1996;334(26):1703–8.
35. Pijls NH, Tonino PA. The CRUX of maximum hyperemia: the last remaining barrier for routine use of fractional flow reserve. JACC Cardiovasc Interv. 2011;4(10):1093–5.
36. Schindler TH, Zhang X-L, Prior JO, Cadenas J, Dahlbom M, Sayre J, Schelbert HR. Assessment of intra- and inter-observer reproducibility of rest and cold-pressor-test stimulated myocardial blood flow with 13N-ammonia and PET. Eur J Nucl Med Mol Imaging. 2007;34:1178–88.
37. Shaw LJ, Berman DS, Maron DJ, et al. Optimal medical therapy with or without percutaneous coronary intervention to reduce ischemic burden: Results from the clinical outcomes utilizing revascularization and aggressive drug evaluation (COURAGE) trial nuclear sub-study. Circulation. 2008;117:1283–91.
38. Tonino PA, De Bruyne B, Pijls NH, et al. Fractional flow reserve versus angiography for guiding percutaneous coronary intervention. N Engl J Med. 2009;360:213–24.
39. Yong ASC, Ho M, Shah MG, Ng MKC, Fearon WF. Coronary microcirculatory resistance is independent of epicardial stenosis. Circ Cardiovasc Interv. 2012;5:103–8.
40. Ziadi MC, deKemp RA, Williams K, Beanlands RSB. Does quantification of myocardial flow reserve using rubidium-82 positron emission tomography facilitate detection of multi-vessel coronary artery disease? J Nucl Cardiol. 2012;19:670–80.
41. Ziadi MC, deKemp RA, Williams K, Beanlands RSB. Impaired myocardial flow reserve on rubidium-82 positron emission tomography imaging predicts adverse outcomes in patients assessed for myocardial ischemia. J Am Coll Cardiol. 2011;58:740–8.

Chapter 13
The Clinical Value of Cardiac PET in Heart Failure

Chi-Lun Ko and Yen-Wen Wu

Abstract Heart failure (HF) is a complex clinical syndrome that results from any structural or functional impairment of ventricular filling or ejection of blood [1]. Approximately 5 million patients in the USA and 15 million patients in Europe have HF. It is the leading cause of hospitalization in elderly people. Despite treatment advances, the mortality rate of HF has increased steadily. More patients are surviving myocardial infarction (MI) due to better standards of care, and consequently this may increase numbers of patients who subsequently develop HF. HF places a significant burden on patients, carers, and healthcare systems.

Limited progress has been made in identifying evidence-based, effective treatments for HF over the last decades. Potential contributors include an incomplete understanding of pathophysiology and poor matching of therapeutic mechanisms.

Positron emission tomography (PET), as a molecular imaging technique, with various tracers allows noninvasive evaluation of contractile function, myocardial perfusion, metabolism, and innervation. Molecular imaging approaches using PET could be further used to evaluate inflammation, angiogenesis, cell death, and ventricular remodeling. It could provide new insights on the chemotherapy-related cardiotoxicity and the roles of stem cell monitoring in living bodies for cell-based therapy from preclinical studies to clinical trials. In conclusion, cardiac PET is a promising tool to understand the physiologic consequences of HF, resulting in early detection of patients with HF at risk, improvement of risk stratification, and

C.-L. Ko, MD
Department of Nuclear Medicine, National Taiwan University Hospital Yun-Lin Branch, Yunlin County, Taiwan

Department of Nuclear Medicine, National Taiwan University Hospital and National Taiwan University College of Medicine, Taipei, Taiwan

Y.-W. Wu, MD, PhD (✉)
Department of Nuclear Medicine, National Taiwan University Hospital and National Taiwan University College of Medicine, Taipei, Taiwan

Cardiology Division of Cardiovascular Medical Center, Far Eastern Memorial Hospital, No.21, Sec.2, Nanya S. Rd., Banciao Dist., New Taipei City 220, Taiwan

Department of Nuclear Medicine, Far Eastern Memorial Hospital, New Taipei City, Taiwan

National Yang-Ming University School of Medicine, Taipei, Taiwan
e-mail: wuyw0502@gmail.com

Y. Kuge et al. (eds.), *Perspectives on Nuclear Medicine for Molecular Diagnosis and Integrated Therapy*, DOI 10.1007/978-4-431-55894-1_13

therapeutic strategy planning and treatment response monitoring. Therefore, in order to give the readers a brief and concise overview, we will mainly review the latest advances in cardiac PET studies in heart failure.

Keywords Heart failure • Positron emission tomography • Myocardial perfusion • Myocardial metabolism • Neuroautonomic system

13.1 Perfusion

13.1.1 Coronary Artery Disease (CAD) and Microvascular Dysfunction

Patients presenting with HF are initially classified based on the etiology of their disease, i.e., ischemic or nonischemic cardiomyopathy. The diagnosis of HF is clear if prior MI is reliably documented. With the wide availability of single-photon emission computed tomography (SPECT) cameras and perfusion tracers, SPECT is currently the preferred imaging modality of cardiac radionuclide imaging with good diagnostic accuracy and prognostic significance.

PET provides better image quality because of higher spatial resolution, less scatter, and fewer attenuation artifacts and may be superior to SPECT with respect to imaging quality, interpretative confidence, and inter-reader agreement. In addition, PET allows quantitative measurement of myocardial perfusion (MP) and metabolism. Cardiac PET with perfusion tracers, such as [^{15}O]-water, [^{13}N]-ammonia, ^{82}rubidium, and [^{18}F]-flurpiridaz [2], allows noninvasive and absolute assessment of regional and global myocardial blood flow (MBF) in ml/min/g. In conjunction with stress, regional and global coronary flow reserve (CFR) can also be calculated, which is the ratio between MBF at peak stress and MBF at rest.

CFR measures not only vasodilator capacity but also endothelial reactivity of the coronary circulation, allowing noninvasive quantitative assessment for patients with diffuse coronary luminal narrowing or microvascular dysfunction.

Coronary microvascular dysfunction is highly prevalent among at-risk individuals and is associated with adverse outcomes regardless of sex, even in the absence of overt coronary atherosclerosis [3]. It may reflect the functional alteration of endothelium, such as hypertension, dyslipidemia, diabetes mellitus, smoking, obesity, or metabolic syndrome, or structural alteration of microangiopathy, myocardial fibrosis, or loss of capillaries. The portion of HF consists predominantly of older age and high prevalence of comorbidities. The systemic pro-inflammatory state may induce coronary endothelial inflammation, microvascular dysfunction, myocardial substrate shift, myocardial and interstitial fibrosis that contribute to high diastolic left ventricular stiffness, and HF development, even with preserved LVEF. The potential roles of myocardial perfusion abnormalities in subjects with cardiovascular risks, metabolic disease, and HF warrant further investigations.

In patients with CAD, a reduced CFR was shown to have prognostic implications, being a more sensitive predictor for cardiac death than was reduced left

ventricular ejection fraction (LVEF). CFR in patients with CAD was found to be also reduced in areas supplied by non-stenotic vessels, suggesting a microvascular component. A recent study showed an association between global CFR and major adverse cardiovascular events (MACE) independently of angiographic CAD prognostic index (CADPI) [4]. This may attribute to diffuse atherosclerosis or microvascular dysfunction. In addition, global CFR also modified the effect of coronary revascularization in terms of event-free survival. These emphasize the utility of cardiac PET in patient risk stratification and the role in decision-making for coronary revascularization.

13.1.2 Transplant Vasculopathy

Cardiac allograft vasculopathy (CAV) is one of the leading causes of late mortality after heart transplantation. It is characterized by the diffuse concentric intima thickening of both epicardial and intramyocardial arteries, which is difficult to be assessed by traditional coronary angiogram. Intravascular ultrasound (IVUS) has been proposed to be the most sensitive method for diagnosis of early CAV. Due to the progressive and diffuse process involving the epicardial and microvascular coronary system, traditional stress myocardial perfusion SPECT frequently underestimates disease severity and extent in patients with CAV. With the absolute-quantitative nature, PET provides a noninvasive way to deal with this problem. A good correlation was observed between plaque burden as determined by IVUS and CFR as assessed by ^{13}N-ammonia PET in recipients with normal coronary angiography findings. Quantitative measurement of myocardial flow using dynamic ^{13}N-ammonia PET is thus clinically feasible [5]. A recent study enrolled 140 posttransplant recipients with median follow-up of 18.2 months; the relative perfusion defects, mean myocardial flow reserve, and mean stress MBF using dipyridamole rubidium-82 PET were significant predictors of adverse outcome [6].

13.2 Sympathetic Innervation

Neurohormonal activation is considered as a compensatory mechanism in HF and maintains perfusion to the heart, yet in the meanwhile is also responsible for the progression of HF. From a long-term point of view, it is associated with cardiac remodeling, progressive impairment of ventricular function, symptoms, and lethal arrhythmia. Despite their critical role in regulation of the heart, local neurohormonal statuses of patients are not routinely and closely monitored in clinical practice. Innervation imaging may provide prognostic information as well as guide selection of therapies. Both a decreased cardiac [^{123}I]-meta-iodobenzylguanidine (MIBG) activity and an increased washout rate are indicative of a poor prognosis in patients with chronic heart failure [7]. Several PET tracers, including

[^{11}C]-meta-hydroxyephedrine (HED), a norepinephrine analog, and [^{11}C]-CGP12177, a beta-adrenoceptor antagonist, not only can be used to visualize global but also regional defects in myocardial sympathetic innervation. A pilot study enrolled 10 patients with dilated cardiomyopathy who underwent PET with [^{11}C]-HED before, acutely and 3 months after cardiac resynchronization (CRT) [8]. It showed CRT improves cardiac sympathetic nerve activity in responders and seems to be more effective in those with functionally preserved neuroautonomic system.

Decreased cardiac beta-adrenoceptor density measured by [^{11}C]-CGP12177 PET was observed in a study of patients with nonischemic cardiomyopathy. In addition the receptor density was significantly correlated with systolic function [9]. Receptor density correlated with [^{123}I]-MIBG washout rate and delayed heart-to-mediastinum (H/M) ratio, but not early H/M ratio. Another study showed that reduced myocardial beta-adrenoceptor density measured by [^{11}C]-CGP12177 early after myocardial infarction is associated with the incidence of congestive heart failure on long-term follow-up [10]. Besides [^{11}C]-labeled tracers, [^{18}F]-N-[3-Bromo-4-(3-fluoro-propoxy)-benzyl]-guanidine (LMI1195), an ^{18}F-labeled analog of [^{123}I]-MIBG SPECT agent, is a new PET tracer retained in the heart through the norepinephrine transporter (NET) and allowing evaluation of the cardiac sympathetic neuronal function by PET imaging [11–13].

13.3 Noninvasive Assessment of Myocardial Metabolism

13.3.1 Myocardial Viability

Myocardial viability, the evaluation of dysfunctional but viable myocardium, can be assessed by several imaging techniques. In conjunction with dobutamine, contractile reserve can be evaluated by either echocardiography or cardiac magnetic resonance imaging (MRI). Delayed contrast-enhanced (DCE) MRI and contrast-enhanced CT can assess scar tissue. Myocardial perfusion SPECT evaluates either cell membrane or mitochondria integrity. [^{18}F]-fluorodeoxyglucose (FDG) can be used to assess glucose metabolism and to differentiate the hibernating myocardium from scar tissue. Dual-isotope simultaneous acquisition (DISA) viability testing, the combination of [^{99m}Tc]-sestamibi and [^{18}F]-FDG SPECT, provides more accurate prediction of post-revascularization functional recovery than thallium-201 [14]. PET using FDG remains the most reliable and noninvasive tool to assess myocardial viability [15] and tends to replace Tl-201 SPECT imaging in centers equipped with a PET/CT camera.

For patients with CAD-associated chronic LV dysfunction, noninvasive detection of myocardial viability is crucial for decision-making of the treatment. Myocardial viability imaging can be used to inform the often difficult clinical decision regarding revascularization in patients with CAD and left ventricular systolic dysfunction, providing data on the potential benefit to balance against the known risks [15]. FDG PET has a higher sensitivity than DCE MRI, but comparable

specificity, in predicting functional recovery [16]. The post hoc subgroup analysis of the PET and Recovery Following Revascularization (PARR-2) trial suggested that FDG PET-guided management reduces the composite of cardiovascular events in patients with ischemic cardiomyopathy in a center with an experienced imaging team [17].

Despite that several studies have emphasized the utility of viability imaging in identifying patients who may benefit from revascularization, a recent meta-analysis shows confusing results [18]. Patients with viable myocardium appear to benefit from revascularization, but the same benefits were observed in patients without viable myocardium. Some suggested this might be resulted from mixed traditional (SPECT and dobutamine echocardiography) and the advanced (MRI and PET) imaging techniques, but this was still not conclusive [19, 20]. A large prospective randomized trial regarding Alternative Imaging Modalities in Ischemic Heart Failure (AIMI-HF) has conducted in 2013 [21], which will complement the results of the Surgical Treatment for Ischemic Heart Failure (STICH) viability substudy and the PET and PARR-2 trial to answer this unsolved issue.

13.3.2 Cardiac Efficiency

[^{11}C]-acetate, a well-known myocardial PET tracer, is directly metabolized into [^{11}C]-acetyl-CoA in mitochondria and enters the Krebs cycle. [^{11}C]-acetate PET imaging provides noninvasive and reproducible measurements of cardiac oxidative metabolism (MVO_2) [22]. Heterogeneously decreased oxidative metabolism was observed in patients with ischemic and nonischemic cardiomyopathy [23]. In chronic HF MI porcine model, myocardial perfusion and oxygen consumption in the remote non-infarcted myocardium were preserved in HF pigs as compared to controls. Global LV work and efficiency were significantly lower in HF than controls and were associated with increased wall stress [24]. It can also be used to evaluate cardiac efficiency under variable conditions, especially after treatments of heart failure. Surgical intervention with LV volume reduction and mitral regurgitation correction significantly improved cardiac efficiency in patients with end-stage heart failure, which is observed in both nonischemic and ischemic etiologies [25].

On the other hand, myocardial oxygen metabolism was increased in patients with aortic stenosis (AS), which was decreased after aortic valve replacement [26]. It is suggested that the increased myocardial oxidative metabolism in AS was largely attributable to the pressure overload of the left ventricle and normalized after unload.

In a study of diastolic heart failure patients, decreased cardiac efficiency is associated with increased LV filling pressure but does not primarily cause diastolic dysfunction or diastolic heart failure in normal hearts [27]. They suggest that improvement of cardiac efficiency may be a target for the treatment of heart failure with preserved ejection fraction (HFpEF).

13.3.3 Cardiac Resynchronization Therapy (CRT)

CRT can correct cardiac dyssynchrony and augment LV systolic function. PET is the only noninvasive imaging technique that can provide information on alternations of myocardial blood flow, glucose utilization, and oxygen consumption. [^{11}C]-acetate PET can also be used to evaluate the efficacy of CRT in patients with severe heart failure [8, 28–31]. CRT could improve cardiac systolic function, but global resting MBF and global MVO_2 are not always altered by CRT, even under stress condition [28]. A more homogeneous myocardial glucose uptake was observed, which implies CRT may induce a more balanced wall stress and energy requirement. Another study demonstrated that decreased oxygen consumption was observed in patients showing good response to CRT. The decrease in oxygen consumption assessed by PET in the early period after CRT is useful to predict improvement of cardiac function and major cardiac events during the first year of follow-up [31].

13.3.4 Chemotherapy-Related Heart Failure

[^{11}C]-acetoacetate, a ketone body tracer, is expected to have some similarities to [^{11}C]-acetate. In mitochondria, acetoacetate is first converted into acetoacetyl-CoA and then into acetyl-CoA. In cytoplasm, acetoacetate can also be directly incorporated into the lipogenesis pathway. Contrary to [^{11}C]-acetate and other MBF PET tracers, [^{11}C]-acetoacetate together with dynamic gated PET imaging was able to identify doxorubicin-induced heart failure at an early stage in a resting state. Thus, [^{11}C]-acetoacetate is promising for the assessment of cardiomyopathy [32].

13.3.5 Metabolic Therapy

Heart failure severity, substrate availability, hormonal status, and coexisting insulin resistance contribute to the metabolic change. Optimizing myocardial energy metabolism has been studied as a novel form of therapy [33]. Metabolic therapy is a promising new avenue for the treatment of heart failure. Suitable targets for therapy include substrate utilization, oxidative phosphorylation, and the availability of high-energy phosphates [34].

Insulin resistance is a recognized phenomenon leading to heart failure. The change in myocardial metabolism can be visualized using PET with metabolic tracers. A prospective study utilized [^{15}O]-water, [^{11}C]-acetate, [^{11}C]-glucose, and [^{11}C]-palmitate PET studies and found that obesity and gender independently modulate MBF and MVO_2. Moreover, gender and obesity may interact in predicting myocardial glucose uptake and insulin sensitivity [35]. FDG PET can also be used in evaluation of the effect of therapy on glucose metabolism. In a transgenic mice model, G protein-coupled receptor kinase 2 inhibition delays the reduction in glucose uptake and protects insulin signaling in the heart, preserving cardiac dimension and function [36].

13.4 Molecular Imaging Approaches of Cardiac Remodeling

13.4.1 Imaging of Matrix Metalloproteinases

The matrix metalloproteinases (MMPs) play a role in physiologic extracellular matrix (ECM) turnover and response to cardiac disease. During the progression of HF, the level of MMPs is increased. The excessive degradation of ECM may result in wall thinning, dilatation, and heart failure. Post-MI myocardial LV remodeling is also associated with changes within the myocardial extracellular matrix and often leads to heart failure. MI results in the activation of the renin-angiotensin-aldosterone system, which in turn results in the activating of MMPs within the heart. Molecular imaging of MMPs has the potential to allow early and serial evaluation of underlying alterations that accompany progression of LV remodeling [37]. The activation of MMPs in infarcted murine myocardium can be imaged by [^{111}In]- and [^{99m}Tc]-labeled single-photon ligands [38]. Several PET tracers have also been synthesized [39]. However, to date there are only limited publications, especially in the field of HF.

13.4.2 Angiogenesis

Angiogenesis occurs in response to ischemia and inflammation being part of the healing process after ischemic tissue injury. [^{18}F]-galacto-RGD allows noninvasive imaging of the expression of $\alpha_v\beta_3$ integrin that is highly expressed in the endothelium of angiogenic vessels. Noninvasive imaging using [^{18}F]-galacto-RGD PET appears promising for the monitoring of therapies aiming to stimulate angiogenesis in ischemic heart disease and preventing the development of HF [40].

13.4.3 Myocardial Inflammation

FDG PET may be useful in the study of inflammatory process since inflammatory cells accumulate glucose. However, a recent study showed some limitations to study the inflammatory process after myocardial infarction even when active uptake of FDG in normal myocardial tissue is suppressed. In the presence of large region of microvascular obstruction, FDG may not reliably and accurately represent the degree of inflammatory cell activity. Even in areas without microvascular obstruction, the degree of inflammation may be underestimated or even overestimated [41].

Besides the usefulness as a molecular target for neuroendocrine tumor imaging, some of the somatostatin receptors are also expressed by activated macrophage. A recent animal study compared [^{68}Ga]-citrate, [^{68}Ga]-DOTATATE, and [^{18}F]-FDG

in a postinfarction mouse model [42]. They conclude that FDG with myocardial suppression is the most practical imaging marker of postinfarction inflammation. However, there are also some studies in human that emphasize the usefulness of the somatostatin receptor imaging in the assessment of sarcoidosis [43] and infarction [44]-related myocardial inflammation. Compared with the nonspecific FDG, this is a new potential biomarker that may be useful in evaluation of myocardial inflammation and predicting cardiac remodeling and progression toward heart failure.

13.5 Conclusions

Advances in the application of cardiac PET may play an increasingly critical role in diagnosis, prognosis, and clinical treatment of cardiovascular diseases. Molecular imaging approaches using PET could evaluate myocardial pathophysiology at different stages of HF. It further provides insights on the HF preventive strategies, tracking patients' clinical status, novel drug therapies, expanding indications for HF therapeutic devices, and gene or cell-based therapies (Fig. 13.1 and Table 13.1).

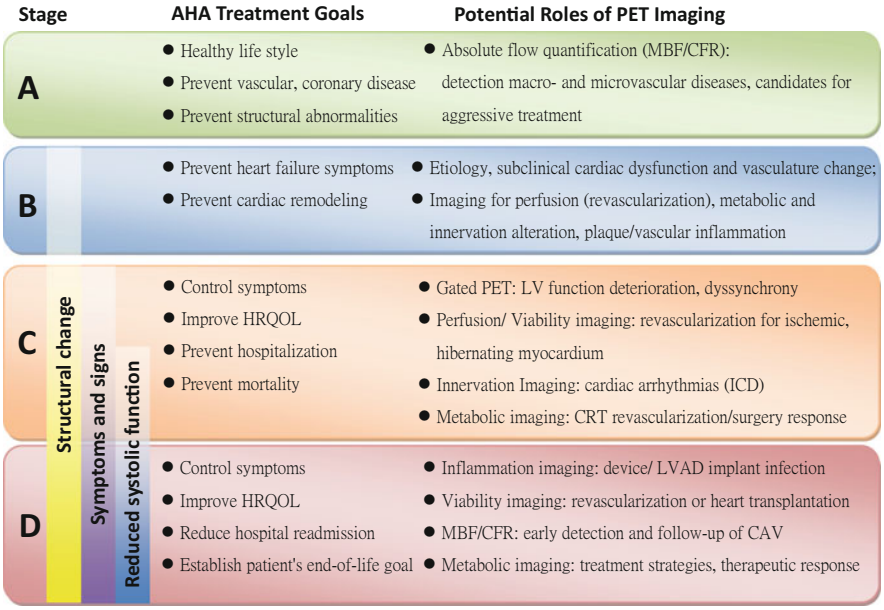

Fig. 13.1 Potential roles of PET imaging in different stages of American College of Cardiology (ACC)/American Heart Association (AHA) classification of heart failure. *CAV* cardiac allograft vasculopathy, *CFR* coronary flow reserve, *HRQOL* health-related quality of life, *ICD* implantable cardioverter defibrillator, *MBF* myocardial blood flow, *LV* left ventricular, *LVAD* left ventricular assist device

Table 13.1 Examples of PET tracers useful in heart failure patients [12, 37, 39]

Substrate	
Glucose	^{18}F-fluorodeoxyglucose
	^{11}C-glucose
Free fatty acid	^{11}C-palmitate
	^{18}F-fluoro-6-thiaheptadecanoic acid
Oxidative metabolism	^{11}C-acetate
Apoptosis	^{18}F-annexin V
Interstitial fibrosis	
Angiotensin-converting enzyme	^{18}F-captopril, ^{18}F-fluorobenzyl-lisinopril
Angiotensin II type 1 receptor	^{11}C-MK-996, ^{11}C-L-159884, ^{11}C-KR31173
Matrix metalloproteinase	^{18}F-FB-ML5
	^{11}C-labeled compounds
Sympathetic innervation	
Presynaptic	^{11}C-meta-hydroxyephedrine (HED)
	^{18}F-fluorodopamine
	^{11}C-epinephrine
	^{11}C-phenylephrine
Postsynaptic	^{11}C-CGP 12177/12388
	^{18}F-fluorocarazolol
Parasympathetic innervation	
Acetylcholine transporter	^{18}F-fluoroethoxybenzovesamicol
Nicotinic receptor	^{18}F-fluoro-A85380
Muscarinic receptor	^{11}C-methylquinuclidiny benzilate

References

1. Yancy CW, Jessup M, Bozkurt B, Butler J, Casey Jr DE, Drazner MH, et al. 2013 ACCF/AHA guideline for the management of heart failure: a report of the American College of Cardiology Foundation/American Heart Association Task Force on Practice Guidelines. J Am Coll Cardiol. 2013;62(16):e147–239. doi:10.1016/j.jacc.2013.05.019.
2. Packard RR, Huang SC, Dahlbom M, Czernin J, Maddahi J. Absolute quantitation of myocardial blood flow in human subjects with or without myocardial ischemia using dynamic

flurpiridaz F 18 PET. J Nucl Med: Off Publ Soc Nucl Med. 2014;55(9):1438–44. doi:10.2967/jnumed.114.141093.
3. Murthy VL, Naya M, Taqueti VR, Foster CR, Gaber M, Hainer J, et al. Effects of sex on coronary microvascular dysfunction and cardiac outcomes. Circulation. 2014;129(24):2518–27. doi:10.1161/circulationaha.113.008507.
4. Taqueti VR, Hachamovitch R, Murthy VL, Naya M, Foster CR, Hainer J, et al. Global coronary flow reserve is associated with adverse cardiovascular events independently of luminal angiographic severity and modifies the effect of early revascularization. Circulation. 2015;131(1):19–27. doi:10.1161/circulationaha.114.011939.
5. Wu YW, Chen YH, Wang SS, Jui HY, Yen RF, Tzen KY, et al. PET assessment of myocardial perfusion reserve inversely correlates with intravascular ultrasound findings in angiographically normal cardiac transplant recipients. J Nucl Med: Off Publ Soc Nucl Med. 2010;51(6):906–12. doi:10.2967/jnumed.109.073833.
6. Mc Ardle BA, Davies RA, Chen L, Small GR, Ruddy TD, Dwivedi G, et al. Prognostic value of rubidium-82 positron emission tomography in patients after heart transplant. Circ Cardiovasc Imaging. 2014;7(6):930–7. doi:10.1161/circimaging.114.002184.
7. Kuwabara Y, Tamaki N, Nakata T, Yamashina S, Yamazaki J. Determination of the survival rate in patients with congestive heart failure stratified by (1)(2)(3)I-MIBG imaging: a meta-analysis from the studies performed in Japan. Ann Nucl Med. 2011;25(2):101–7. doi:10.1007/s12149-010-0452-0.
8. Martignani C, Diemberger I, Nanni C, Biffi M, Ziacchi M, Boschi S, et al. Cardiac resynchronization therapy and cardiac sympathetic function. Eur J Clin Investig. 2015;45(8):792–9. doi:10.1111/eci.12471.
9. Tsukamoto T, Morita K, Naya M, Inubushi M, Katoh C, Nishijima K, et al. Decreased myocardial beta-adrenergic receptor density in relation to increased sympathetic tone in patients with nonischemic cardiomyopathy. J Nucl Med: Off Publ Soc Nucl Med. 2007;48(11):1777–82. doi:10.2967/jnumed.107.043794.
10. Gaemperli O, Liga R, Spyrou N, Rosen SD, Foale R, Kooner JS, et al. Myocardial beta-adrenoceptor down-regulation early after infarction is associated with long-term incidence of congestive heart failure. Eur Heart J. 2010;31(14):1722–9. doi:10.1093/eurheartj/ehq138.
11. Yu M, Bozek J, Lamoy M, Guaraldi M, Silva P, Kagan M, et al. Evaluation of LMI1195, a novel 18F-labeled cardiac neuronal PET imaging agent, in cells and animal models. Circ Cardiovasc Imaging. 2011;4(4):435–43. doi:10.1161/circimaging.110.962126.
12. Werner RA, Rischpler C, Onthank D, Lapa C, Robinson S, Sammnick S, et al. Retention Kinetics of the 18F-labeled Sympathetic Nerve PET Tracer LMI1195: Comparison with 11C-HED and 123I-MIBG. J Nucl Med: Off Publ Soc Nucl Med. 2015. doi:10.2967/jnumed.115.158493.
13. Chen X, Werner RA, Javadi MS, Maya Y, Decker M, Lapa C, et al. Radionuclide imaging of neurohormonal system of the heart. Theranostics. 2015;5(6):545–58. doi:10.7150/thno.10900.
14. Wu YW, Huang PJ, Lee CM, Ho YL, Lin LC, Wang TD, et al. Assessment of myocardial viability using F-18 fluorodeoxyglucose/Tc-99m sestamibi dual-isotope simultaneous acquisition SPECT: comparison with Tl-201 stress-reinjection SPECT. J Nucl Cardiol. 2005;12(4):451–9. doi:10.1016/j.nuclcard.2005.04.007.
15. Schinkel AF, Poldermans D, Elhendy A, Bax JJ. Assessment of myocardial viability in patients with heart failure. J Nucl Med: Off Publ Soc Nucl Med. 2007;48(7):1135–46. doi:10.2967/jnumed.106.038851.
16. Allman KC, Shaw LJ, Hachamovitch R, Udelson JE. Myocardial viability testing and impact of revascularization on prognosis in patients with coronary artery disease and left ventricular dysfunction: a meta-analysis. J Am Coll Cardiol. 2002;39(7):1151–8.
17. Abraham A, Nichol G, Williams KA, Guo A. deKemp RA, Garrard L et al. 18F-FDG PET imaging of myocardial viability in an experienced center with access to 18F-FDG and integration with clinical management teams: the Ottawa-FIVE substudy of the PARR 2 trial. J Nucl Med: Off Publ Soc Nucl Med. 2010;51(4):567–74. doi:10.2967/jnumed.109.065938.

18. Orlandini A, Castellana N, Pascual A, Botto F, Cecilia Bahit M, Chacon C, et al. Myocardial viability for decision-making concerning revascularization in patients with left ventricular dysfunction and coronary artery disease: a meta-analysis of non-randomized and randomized studies. Int J Cardiol. 2015;182:494–9. doi:10.1016/j.ijcard.2015.01.025.
19. Srichai MB, Jaber WA. Viability by MRI or PET would have changed the results of the STICH trial. Prog Cardiovasc Dis. 2013;55(5):487–93. doi:10.1016/j.pcad.2013.01.005.
20. Asrani NS, Chareonthaitawee P, Pellikka PA. Viability by MRI or PET would not have changed the results of the STICH trial. Prog Cardiovasc Dis. 2013;55(5):494–7. doi:10.1016/j.pcad.2012.09.004.
21. O'Meara E, Mielniczuk LM, Wells GA. deKemp RA, Klein R, Coyle D et al. Alternative Imaging Modalities in Ischemic Heart Failure (AIMI-HF) IMAGE HF Project I-A: study protocol for a randomized controlled trial. Trials. 2013;14:218. doi:10.1186/1745-6215-14-218.
22. Nesterov SV, Turta O, Han C, Maki M, Lisinen I, Tuunanen H, et al. C-11 acetate has excellent reproducibility for quantification of myocardial oxidative metabolism. Eur Heart J Cardiovasc Imaging. 2015;16(5):500–6. doi:10.1093/ehjci/jeu289.
23. Wu YW, Naya M, Tsukamoto T, Komatsu H, Morita K, Yoshinaga K, et al. Heterogeneous reduction of myocardial oxidative metabolism in patients with ischemic and dilated cardiomyopathy using C-11 acetate PET. Circ J: Off J Jpn Circ Soc. 2008;72(5):786–92.
24. Tarkia M, Stark C, Haavisto M, Kentala R, Vahasilta T, Savunen T, et al. Cardiac remodeling in a new pig model of chronic heart failure: Assessment of left ventricular functional, metabolic, and structural changes using PET, CT, and echocardiography. J Nucl Cardiol. 2015. doi:10.1007/s12350-015-0068-9.
25. Sugiki T, Naya M, Manabe O, Wakasa S, Kubota S, Chiba S, et al. Effects of surgical ventricular reconstruction and mitral complex reconstruction on cardiac oxidative metabolism and efficiency in nonischemic and ischemic dilated cardiomyopathy. J Am Coll Cardiol Img. 2011;4(7):762–70. doi:10.1016/j.jcmg.2011.04.010.
26. Naya M, Chiba S, Iwano H, Yamada S, Katoh C, Manabe O, et al. Myocardial oxidative metabolism is increased due to hemodynamic overload in patients with aortic valve stenosis: assessment using 11C-acetate positron emission tomography. Eur J Nucl Med Mol Imaging. 2010;37(12):2242–8. doi:10.1007/s00259-010-1540-z.
27. Hasegawa S, Yamamoto K, Sakata Y, Takeda Y, Kajimoto K, Kanai Y, et al. Effects of cardiac energy efficiency in diastolic heart failure: assessment with positron emission tomography with 11C-acetate. Hypertens Res. 2008;31(6):1157–62. doi:10.1291/hypres.31.1157.
28. Henneman MM, van der Wall EE, Ypenburg C, Bleeker GB, van de Veire NR, Marsan NA, et al. Nuclear imaging in cardiac resynchronization therapy. J Nucl Med: Off Publ Soc Nucl Med. 2007;48(12):2001–10. doi:10.2967/jnumed.107.040360.
29. Ypenburg C, Bax JJ. The role of positron emission tomography in evaluation of alterations in cardiac efficiency after cardiac resynchronization therapy. J Cardiovasc Electrophysiol. 2008;19(2):133–5. doi:10.1111/j.1540-8167.2007.01032.x.
30. Kitaizumi K, Yukiiri K, Masugata H, Shinomiya K, Ohara M, Takinami H, et al. Positron emission tomographic demonstration of myocardial oxidative metabolism in a case of left ventricular restoration after cardiac resynchronization therapy. Circ J: Off J Jpn Circ Soc. 2008;72(11):1900–3.
31. Kitaizumi K, Yukiiri K, Masugata H, Takinami H, Iwado Y, Noma T, et al. Acute improvement of cardiac efficiency measured by 11C-acetate PET after cardiac resynchronization therapy and clinical outcome. Int J Cardiovasc Imaging. 2010;26(3):285–92. doi:10.1007/s10554-009-9549-8.
32. Croteau E, Tremblay S, Gascon S, Dumulon-Perreault V, Labbe SM, Rousseau JA, et al. [(11)C]-Acetoacetate PET imaging: a potential early marker for cardiac heart failure. Nucl Med Biol. 2014;41(10):863–70. doi:10.1016/j.nucmedbio.2014.08.006.
33. Tuunanen H, Ukkonen H, Knuuti J. Myocardial fatty acid metabolism and cardiac performance in heart failure. Curr Cardiol Rep. 2008;10(2):142–8.

34. Knaapen P, Knuuti J, van Rossum AC. The failing heart. N Engl J Med. 2007;356(24):2545. author reply 6.
35. Peterson LR, Soto PF, Herrero P, Mohammed BS, Avidan MS, Schechtman KB, et al. Impact of gender on the myocardial metabolic response to obesity. J Am Coll Cardiol Img. 2008;1 (4):424–33. doi:10.1016/j.jcmg.2008.05.004.
36. Ciccarelli M, Chuprun JK, Rengo G, Gao E, Wei Z, Peroutka RJ, et al. G protein-coupled receptor kinase 2 activity impairs cardiac glucose uptake and promotes insulin resistance after myocardial ischemia. Circulation. 2011;123(18):1953–62. doi:10.1161/circulationaha.110.988642.
37. Shirani J, Dilsizian V. Molecular imaging targets of cardiac remodeling. Curr Cardiol Rep. 2009;11(2):148–54.
38. Su H, Spinale FG, Dobrucki LW, Song J, Hua J, Sweterlitsch S, et al. Noninvasive targeted imaging of matrix metalloproteinase activation in a murine model of postinfarction remodeling. Circulation. 2005;112(20):3157–67. doi:10.1161/circulationaha.105.583021.
39. Matusiak N, van Waarde A, Bischoff R, Oltenfreiter R, van de Wiele C, Dierckx RA, et al. Probes for non-invasive matrix metalloproteinase-targeted imaging with PET and SPECT. Curr Pharm Des. 2013;19(25):4647–72.
40. Higuchi T, Bengel FM, Seidl S, Watzlowik P, Kessler H, Hegenloh R, et al. Assessment of alphavbeta3 integrin expression after myocardial infarction by positron emission tomography. Cardiovasc Res. 2008;78(2):395–403. doi:10.1093/cvr/cvn033.
41. Prato FS, Butler J, Sykes J, Keenliside L, Blackwood KJ, Thompson RT, et al. Can the inflammatory response be evaluated using 18F-FDG within zones of microvascular obstruction after myocardial infarction? J Nucl Med: Off Publ Soc Nucl Med. 2015;56(2):299–304. doi:10.2967/jnumed.114.147835.
42. Thackeray JT, Bankstahl JP, Wang Y, Korf-Klingebiel M, Walte A, Wittneben A, et al. Targeting post-infarct inflammation by PET imaging: comparison of (68)Ga-citrate and (68)Ga-DOTATATE with (18)F-FDG in a mouse model. Eur J Nucl Med Mol Imaging. 2015;42(2):317–27. doi:10.1007/s00259-014-2884-6.
43. Reiter T, Werner RA, Bauer WR, Lapa C. Detection of cardiac sarcoidosis by macrophage-directed somatostatin receptor 2-based positron emission tomography/computed tomography. Eur Heart J. 2015. doi:10.1093/eurheartj/ehv278.
44. Lapa C, Reiter T, Li X, Werner RA, Samnick S, Jahns R, et al. Imaging of myocardial inflammation with somatostatin receptor based PET/CT – A comparison to cardiac MRI. Int J Cardiol. 2015;194:44–9. doi:10.1016/j.ijcard.2015.05.073.

Chapter 14
Emerging Trends and Future Perspective of Novel Cardiac SPECT Technology

Masao Miyagawa, Yoshiko Nishiyama, Hayato Ishimura, Rami Tashiro, Kana Ide, and Teruhito Mochizuki

Abstract In response to concerns about overuse and increasing radiation exposure of myocardial perfusion imaging, nuclear medicine societies have declared statements aimed at lowering its radiation dose and costs. Simultaneously, two vendors have launched novel SPECT scanners with solid-state semiconductor detectors. Discovery NM 530c and D-SPECT utilize the same cadmium zinc telluride (CZT) detectors with a different combination of high-sensitivity multi-pinhole or parallel-hole collimator which focuses on the heart. The physical performance of those is dramatically higher than that of conventional Anger cameras; however, 2 CZT cameras are inherently different.

Although ^{99m}Tc-labeled myocardial perfusion tracers might not be ideal agents, estimation of absolute myocardial blood flow or myocardial flow reserve (MFR) using dynamic CZT SPECT is a challenging subject and attracts a great deal of interest in the field. Thus, novel software which allows automatic calculation of MFR index with dynamic CZT SPECT is currently under development and validated in our institution. This technology will hold promise if the several issues can be solved through future studies.

Keywords Cadmium zinc telluride • Cardiac SPECT • Coronary flow reserve • Effective dose • Dynamic imaging

14.1 Introduction

The overall utilization for stress myocardial perfusion imaging (MPI) reached its height in 2006 with over 10 million studies and Medicare payment over 1 billion dollars [1]. The National Council on Radiation Protection and Measurements

M. Miyagawa, MD, Ph.D. (✉) • Y. Nishiyama, MD, Ph.D. • H. Ishimura, RT • R. Tashiro, MD, Ph.D. • K. Ide, MD, Ph.D. • T. Mochizuki, MD, Ph.D.
Department of Radiology, Ehime University Graduate School of Medicine, Shitsukawa, Toon-city, Ehime 791-0295, Japan
e-mail: miyagawa@m.ehime-u.ac.jp

Y. Kuge et al. (eds.), *Perspectives on Nuclear Medicine for Molecular Diagnosis and Integrated Therapy*, DOI 10.1007/978-4-431-55894-1_14

reported that since the early 1980s, a six-fold increase in radiation exposure to the US population from medical procedures [2] emphasizes that more than 10 % of the entire radiation burden was related to MPI [3]. In response to these concerns, professional societies have declared statements aimed at lowering its radiation dose and costs [4, 5].

Simultaneously, vendors have developed dedicated cardiac SPECT scanners with solid-state semiconductor detectors in order to do something about radiation dose and long imaging time. Two vendors have introduced novel scanners: Discovery NM 530c, (D530c); GE Healthcare and D-SPECT; and Spectrum Dynamics utilizing the same cadmium zinc telluride (CZT) detectors, with a different combination of high-sensitivity multi-pinhole or parallel-hole collimators which focuses on the myocardium [6, 7]. More than 300 of such cardiac CZT SPECT scanners are currently available in the world, and the number is increasing by more than 100 per year.

Firstly, we focus on the latest advances in MPI procedures which ought to be able to maximize the value of SPECT cameras with CZT detectors. Secondly, we try to develop a novel software for calculating the myocardial flow reserve (MFR) index using these cameras and to validate its utility for screening patients with multi-vessel coronary artery disease (CAD).

14.2 Materials and Methods

Initially, we conducted a comparative study using ^{99m}Tc line-source phantoms with and without photon scattering caused by water in the cylinder [8]. D530c had a more than two-fold spatial resolution than did the conventional Anger camera with a dual detector (Infinia; GE Healthcare). We also found that a D530c has better energy resolution compared to Infinia, which is as narrow as 5 %. Therefore, energy window width could be narrowed enough to be feasible for performing dual radioisotope simultaneous SPECT with ^{99m}Tc-tetrofosmin and ^{123}I-BMIPP [9].

MPI protocol for routine clinical practice of our institution at present is summarized in Fig. 14.1. We adopt a stress-first one-day protocol with ^{99m}Tc-perfusion tracers. CZT camera has a 5-times higher sensitivity; therefore, patients are given an injection of only 3 MBq/kg body weight (4–5 mCi) of ^{99m}Tc-perfusion tracers at peak stress. Supine and prone imaging with 5 min each is routinely performed [10]. Same-day rest imaging was performed after 9 MBq/kg of tracer injection. If we apply a strategy of stress-only protocol to our routine clinical practice, we will get further reduction in the effective radiation dose of patients and higher laboratory throughput.

Dynamic MPI starting with the bolus administration of ^{99m}Tc-perfusion tracers as described above was also performed during adenosine stress and at rest using the CZT camera. We intravenously injected saline followed by radionuclide, using an

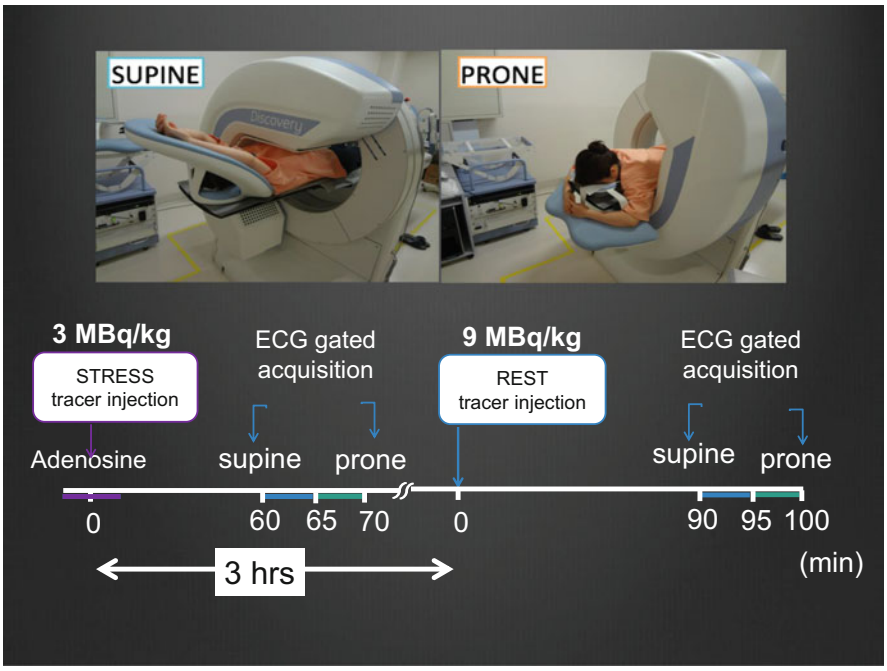

Fig. 14.1 We adopt a stress/rest one-day protocol with Tc-99m perfusion radiotracers. Supine and prone positioning are routinely performed. The total effective dose ranged 3.4–6.7 mSv. Stress-only MPI can be performed with the effective dose averaging 1 mSv

automatic injector at a constant rate of 1 milliliter per second for 30 s (Fig. 14.2). Before dynamic imaging, we carefully detected the border of the heart by chest percussion or test injection of 0.5 mCi of tracers in order to adjust the position of the heart appropriately in the quality field of view [11]. The interval between stress and rest imaging was 3 h and a 30-s pre-scan count was subtracted from the dynamic data at rest. 10-min dynamic SPECT data with list mode acquisition were reconstructed using a maximum likelihood expectation maximization (MLEM) algorithm with 40–50 iterations. We generated 200 3-D volumes integrating 3-s time frames in the course of 600 s. Routine MPI were also acquired thereafter.

The software allows the automatic edge detection of volume of interest for the blood pool in the left ventricle and the myocardium. Global time-activity curves were fitted to a one-tissue two-compartment kinetic model (2-com), a Patlak plot analysis (PPA), and a dose uptake ratio of MPI (DUR) with input function. K1 and K2 were calculated for the stress and rest images. MFR index was calculated as follows: MFR index = K1 stress/K1 at rest.

The validation study included 64 consecutive pts who underwent CZT SPECT and invasive coronary angiography within 2 weeks (35 males, 67 ± 10 years old). 15 pts had single-vessel CAD, and 22 pts had multi-vessel CAD (10 had two-vessel and 12 had three-vessel CAD) and 27 pts with no significant coronary stenosis less than 70 %.

Fig. 14.2 For bolus administration of tracer, we intravenously injected saline, using an automatic injector at a constant rate of 1 milliliter per second for 30 s. We started the dynamic data acquisition just after the bolus injection

14.3 Results and Discussion

14.3.1 Reduction in Injection Dose of Radiopharmaceuticals

The introduction of CZT cameras has opened the possibility of reducing radiation dose of SPECT MPI. Oddstig et al. [12] reported that they performed a 1-day ^{99m}Tc-tetrofosmin stress-rest protocol using D530c in 150 patients who were divided into three subgroups (50 patients in each group) with 4, 3, and 2.5 MBq/kg body weight of administered activity in the stress MPI, respectively. The total effective dose (stress and rest) decreased from 9.3 mSv in the 4 MBq/kg group to 5.8 mSv in the 2.5 MBq/kg group. The image acquisition times for 2.5 MBq/kg were 8 and 5 min (stress and rest, respectively) compared to 15 min for each when using conventional SPECT. The average image quality for the stress and the rest showed no statistically significant difference among the 4, 3, and 2.5 MBq/kg groups.

Starting the MPS protocol with examination at stress and analyzing the stress images before deciding of the need for rest examination (i.e., to say "stress-only protocol") reduce the effective dose [13, 14]. The effective dose was no more than 1.4 mSv for a patient receiving 2.5 MBq/kg, who underwent the stress-only

protocol. The total effective radiation dose ranged 3 to 6 mSv with the stress-rest protocol in our institution. If applied, stress-only protocol would be performed with the effective dose averaging 1 mSv. Novel CZT technology can considerably decrease the effective dose for MPI with preserved high image quality.

Moreover, the high sensitivity of D530c allows for a shorter acquisition time; actually, 5 min is sufficient for QGS in the clinical setting. Although CZT detectors are higher in cost, they have been shown to provide an eight- to ten-fold increase in sensitivity, coupled with a two-fold improvement in spatial resolution, and higher energy resolution enabling a significant reduction in imaging time and dose of isotopes and a dual radionuclide simultaneous SPECT with ^{99m}Tc and ^{123}I [6, 7].

Imbert et al. also conducted analyses of phantom and human SPECT images, comparing the D530c and D-SPECT CZT cameras with Anger cameras, and reported that the physical performance of CZT cameras is dramatically higher than that of Anger cameras; however, 2 CZT cameras are inherently different. Spatial resolution and contrast-to-noise ratio are better with the Discovery NM 530c, whereas detection sensitivity is markedly higher with the D-SPECT [15].

14.3.2 Attempts to Estimate Coronary Flow Reserve Using CZT SPECT

At present, coronary flow reserve (CFR) has been mostly replaced by FFR primarily due to its technical simplicity in the catheterization lab. In contrast, in the noninvasive field, PET-derived CFR is an emerging index used for improving both the diagnosis and risk stratification in patients with suspected CAD. And with the increased use, reliable evidences have been suggested that CFR is a powerful independent predictor of cardiac events and mortality [16–19].

In parallel to the work on these PET studies, some studies have continuously reported that using first-pass planar scintigraphy in humans [20–24] or dynamic SPECT in animals [25] provides evidences that the estimates of CFR can be also derived from conventional SPECT MPI. Although fair agreements have been noted between CFR estimated by SPECT and PET or intracoronary Doppler flow studies, they also highlighted the limitations of conventional gamma camera for the dynamic data collection during rapidly changing radiotracer concentrations [26].

The CZT cameras provide higher temporal and spatial resolution. Dynamic SPECT imaging during the first pass of a tracer was attained with the use of these cameras. From the list data, time-activity curves (TAC) would be generated for the left ventricular cavity (input function) and for myocardial tissue (output function) during stress and rest. Ben-Haim et al. [27] firstly reported the feasibility of dynamic ^{99m}Tc-MIBI SPECT and quantitation of global and regional CFRs using the D-SPECT. They calculated CFR index as the ratio of the stress and rest K1 values. Global CFR index was higher in patients with normal MPI than in patients

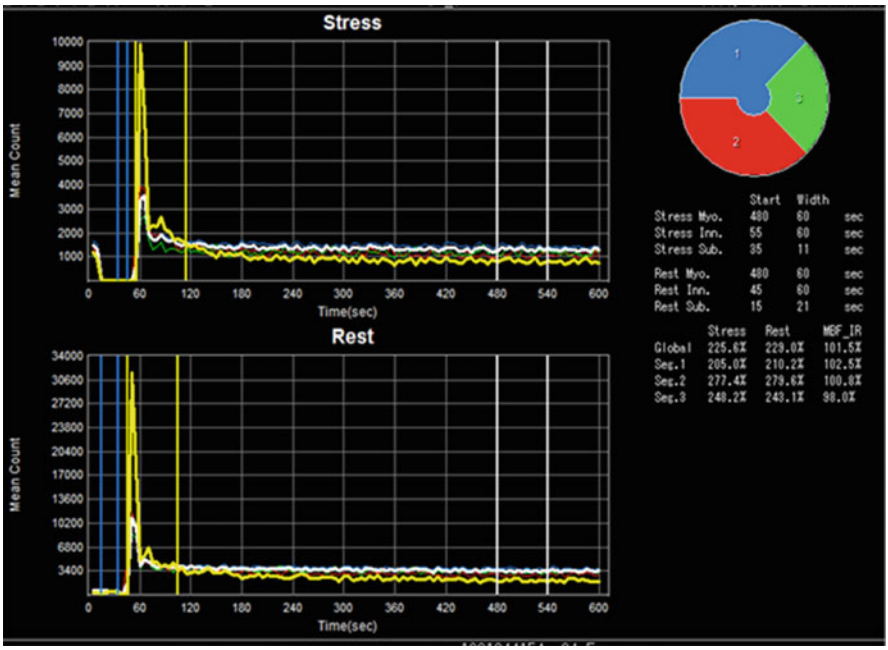

Fig. 14.3 Dynamic acquisition images were transferred to a workstation for analysis using a novel software. It allows an automatic definition of a volume of interest (VOI) for the blood pool in the left ventricle and the left ventricular myocardium. The time-activity curve (TAC) can be extracted by averaging the signal intensity in the VOI in each time frame and then expressed in counts per mm^3/s

with abnormal MPI. The CFR index was lower in territories supplied by stenotic coronary arteries than in non-stenotic arteries.

Novel software is currently under development in our institution [28]. TACs by dynamic ^{99m}Tc-tetrofosmin SPECT using the D530c during adenosine stress and rest are shown in Fig. 14.3. TAC can be extracted by averaging the signal intensity in the volume of interest (VOI) in each time frame and then expressed in counts per cubic mm^3/s. Global TAC was fitted to a 2-com model with input functions which was served by the blood pool curves. In the validation study, Global MFR index estimated by the 2-com model is significantly lower in patients with multi-vessel disease, than those without the disease. In addition, MFR index in the segments of vascular territories with significant coronary stenosis is significantly lower than those without coronary stenosis.

Most recently, Wells et al. applied the D530c to a study with a pig model for quantitation of absolute myocardial blood flow (MBF) using common perfusion tracers as ^{99m}Tc-MIBI, ^{99m}Tc-tetrofosmin, and thallium-201 [29]. Dynamic images were reconstructed with CT-based attenuation correction and energy window-based scatter correction and then processed with kinetic analysis using a 1-tissue 2-com model to obtain the uptake rate constant K1 as a function of microsphere MBF. Converting K1 back to MBF using the measured extraction fractions produced

accurate values and good correlations with microsphere MBF. They have demonstrated that dynamic SPECT by the CZT camera may be feasible to estimate absolute MBF.

14.3.3 Advantages and Disadvantages of the Measurement of CFR with SPECT

At the current moment, PET plays a major role in accurate estimation of MBF or CFR. However, it has limited value for routine clinical studies because of its higher cost and more complicated procedures, including the production of short-half-lived positron tracers by in-house cyclotrons. Therefore, the advantage of SPECT-measured technique utilizing common technetium-99 m perfusion tracers is that it would increase the utility of CFR measurement in the clinical setting with a much smaller financial cost.

On the other hand, the disadvantage of quantifying CFR with SPECT may be the underestimation of the CFR value, compared to that with PET. The reasons for this underestimation could be mainly due to the limited extraction of technetium-99 m perfusion tracers at high flow rates, at which the extraction of the tracer becomes limited by membrane transport [26].

14.4 Conclusions

We need to explore patient-centered, radiation exposure-controlled, and appropriately designed protocols which do not sacrifice image quality or diagnostic accuracy of the new modality. Although ^{99m}Tc-labeled radiotracers might not be ideal flow agents, estimation of absolute MBF or CFR using dynamic CZT SPECT is challenging and of great interest. This technology will hold great promise if the several issues can be solved through future studies.

References

1. McNulty EJ, Hung Y, Almers LM, Go AS, Yeh RW. Population trends from 2000–2011 in nuclear myocardial perfusion imaging use. JAMA. 2014;311:1248–9.
2. National Council on Radiation Protection and Measurements. Report No. 160, Ionizing Radiation Exposure of the Population of the United States: National Council on Radiation Protection and Measurements; 2009.
3. Einstein AJ. Effects of radiation exposure from cardiac imaging: how good are the data? J Am Coll Cardiol. 2012;59:553–65.
4. Cerqueira MD, Allman KC, Ficaro EP, et al. Recommendations for reducing radiation exposure in myocardial perfusion imaging. J Nucl Cardiol. 2010;17:709–18.
5. DePuey EG, Mahmarian JJ, Miller TD, et al. Patient-centered imaging, ASNC Preferred Practice Statement. J Nucl Cardiol. 2012;19:185–215.
6. Bocher M, Blevis IM, Tsukerman L, Shrem Y, Kovalski G, Volokh L. A fast cardiac gamma camera with dynamic SPECT capabilities: design, system validation and future potential. Eur J Nucl Med Mol Imaging. 2010;37:1887–902.
7. Patton J, Slomka P, Germano G, Berman D. Recent technologic advances in nuclear cardiology. J Nucl Cardiol. 2007;14:501–13.
8. Takahashi Y, Miyagawa M, Nishiyama Y, Ishimura H, Mochizuki T. Performance of a semiconductor SPECT system: comparison with a conventional Anger-type SPECT instrument. Ann Nucl Med. 2013;27:11–6.
9. Takahashi Y, Miyagawa M, Nishiyama Y, Kawaguchi N, Ishimura H, Mochizuki T. Dual radioisotopes simultaneous SPECT of ^{99m}Tc-tetrofosmin and ^{123}I-BMIPP using a semiconductor detector. Asia Oceania J Nucl Med Biol. 2014;3:43–9.
10. Nishiyama Y, Miyagawa M, Kawaguchi N, et al. Combined supine and prone myocardial perfusion single-photon emission computed tomography with a cadmium zinc telluride camera for detection of coronary artery disease. Circ J. 2014;78:1169–75.
11. Hindorf C, Oddstig J, Hedeer F, Hansson MJ, Jögi J, Engblom H. Importance of correct patient positioning in myocardial perfusion SPECT when using a CZT camera. J Nucl Cardiol. 2014;21:695–702.
12. Oddstig J, Hedeer F, Jogi J, Carlsson M, Hindorf C, Engblom H. Reduced administered activity, reduced acquisition time, and preserved image quality for the new CZT camera. J Nucl Cardiol. 2013;20:38–44.
13. Duvall WL, Wijetunga MN, Klein TM, et al. Stress-only Tc-99m myocardial perfusion imaging in an Emergency Department Chest Pain Unit. J Emerg Med. 2011;42:642–50.
14. Einstein AJ, Johnson LL, DeLuca AJ, et al. Radiation dose and prognosis of ultra-low-dose stress-first myocardial perfusion SPECT in patients with chest pain using a high-efficiency camera. J Nucl Med. 2015;56:545–51.
15. Imbert L, Poussier S, Franken PR, et al. Compared performance of high-sensitivity cameras dedicated to myocardial perfusion SPECT: a comprehensive analysis of phantom and human images. J Nucl Med. 2012;53:1897–903.
16. Yoshinaga K, Chow BJ, Williams K, et al. What is the prognostic value of myocardial perfusion imaging using rubidium-82 positron emission tomography? J Am Coll Cardiol. 2006;48:1029–39.
17. Herzog BA, Husmann L, Valenta I, et al. Long-term prognostic value of ^{13}N ammonia myocardial perfusion positron emission tomography added value of coronary flow reserve. J Am Coll Cardiol. 2009;54:150–6.
18. Murthy VL, Naya M, Foster CR, et al. Improved cardiac risk assessment with noninvasive measures of coronary flow reserve. Circulation. 2011;124:2215–24.
19. Naya M, Murthy VL, Taqueti VR, et al. Preserved coronary flow reserve effectively excludes high-risk coronary artery disease on angiography. J Nucl Med. 2014;55:248–55.

20. Taki J, Fujino S, Nakajima K, et al. Tc-99m retention characteristics during pharmacological hyperemia in human myocardium: comparison with coronary flow reserve measured by Doppler flowire. J Nucl Med. 2001;42:1457–63.
21. Sugihara H, Yonekura Y, Kataoka K, Fukai D, Kitamura N, Taniguchi Y. Estimation of coronary flow reserve with the use of dynamic planar and SPECT images of Tc-99m tetrofosmin. J Nucl Cardiol. 2001;8:575–9.
22. Ito Y, Katoh C, Noriyasu K, et al. Estimation of myocardial blood flow and myocardial flow reserve by 99mTc-sestamibi imaging: comparison with the results of O-15 H_2O PET. Eur J Nucl Med Mol Imaging. 2003;30:281–7.
23. Storto G, Cirillo P, Vicario ML, et al. Estimation of coronary flow reserve by Tc-99m sestamibi imaging in patients with coronary artery disease: comparison with the results of intracoronary Doppler technique. J Nucl Cardiol. 2004;11:682–8.
24. Daniele S, Nappi C, Acampa W, et al. Incremental prognostic value of coronary flow reserve assessed with single-photon emission computed tomography. J Nucl Cardiol. 2011;18:612–9.
25. Iida H, Eberl S, Kim KM, et al. Absolute quantitation of myocardial blood flow with ^{201}Tl and dynamic SPECT in canine: optimization and validation of kinetic modeling. Eur J Nucl Med Mol Imaging. 2008;35:896–905.
26. Petretta M, Soricelli A, Storto G, Cuocolo A. Assessment of coronary flow reserve using single photon emission computed tomography with technetium 99m-labeled tracers. J Nucl Cardiol. 2008;15:456–65.
27. Ben-Haim S, Murthy VL, Breault C, et al. Quantification of myocardial perfusion reserve using dynamic SPECT imaging in humans: a feasibility study. J Nucl Med. 2013;54:873–9.
28. Miyagawa M, Nishiyama Y, Kawaguchi N, et al. Estimation of myocardial flow reserve using a cadmium-zinc telluride (CZT) SPECT in patients with multi-vessel coronary artery disease. J Nucl Med 2013:54;Supplement 157P.
29. Wells RG, Timmins R, Klein R, et al. Dynamic SPECT measurement of absolute myocardial blood flow in a porcine model. J Nucl Med. 2014;55:1685–91.

Chapter 15
Right Ventricular Metabolism and Its Efficiency

Clinical Aspects and Future Directions

Keiichiro Yoshinaga, Hiroshi Ohira, Ichizo Tsujino, Osamu Manabe, Takahiro Sato, Chietsugu Katoh, Katsuhiko Kasai, Yuuki Tomiyama, Masaharu Nishimura, and Nagara Tamaki

Abstract *Background*: Elevated pulmonary arterial pressure may increase right ventricular (RV) oxidative metabolism in patients with pulmonary hypertension (PH) and heart failure (HF). ^{11}C- acetate positron emission tomography (PET) can be used to measure RV oxidative metabolism noninvasively. The combination of RV oxidative metabolism and cardiac work, as estimated by cardiac magnetic resonance imaging (CMR), indicates RV efficiency and can provide new insights. However, the clinical importance of these markers has not been fully studied. The purpose of this study was to investigate the possible impacts of these markers in patients with PH through ^{11}C-acetate PET.

Methods: Ventricular function was assessed using magnetic resonance imaging (MRI). Dynamic ^{11}C-acetate PET was used to simultaneously measure RV and

K. Yoshinaga, MD, Ph.D., FACC (✉)
Department of Nuclear Medicine, Hokkaido University Graduate School of Medicine, Kita15 Nishi7, Kita-Ku, Sapporo 060-8638, Hokkaido, Japan

Molecular Imaging Research Center, National Institute of Radiological Sciences, 4-9-1 Anagawa, Inage-Ku, Chiba 263-8555, Japan
e-mail: kyoshi@nirs.go.jp

H. Ohira, MD, Ph.D. • I. Tsujino, MD, Ph.D. • T. Sato, MD, Ph.D. • M. Nishimura, MD, Ph.D.
First Department of Medicine, Hokkaido University Graduate School of Medicine, Sapporo, Japan

O. Manabe, MD, Ph.D. • Y. Tomiyama, MSc
Department of Nuclear Medicine, Hokkaido University Graduate School of Medicine, Sapporo, Japan

C. Katoh, MD, Ph.D. • K. Kasai, MSc
Hokkaido University Graduate School of Health Sciences, Sapporo, Japan

N. Tamaki, MD, Ph.D.
Department of Nuclear Medicine, Hokkaido University Graduate School of Medicine, Sapporo, Japan

Department of Nuclear Medicine, Graduate School of Medicine, Hokkaido University, Sapporo, Japan

Y. Kuge et al. (eds.), *Perspectives on Nuclear Medicine for Molecular Diagnosis and Integrated Therapy*, DOI 10.1007/978-4-431-55894-1_15

left ventricular (LV) oxidative metabolism (k_{mono}). The RV myocardial work per oxygen consumption index was calculated as follows: [RV stroke volume index (SVI)/RV k_{mono}]. PH patients who had additional or increased doses of PH-specific vasodilator(s), based on the joint guidelines of the European Society of Cardiology (ESC) and European Respiratory Society (ERS) for the diagnosis and management of PH, were compared with five PH patients who had no treatment modification (control group).

Results: PH patients showed higher RV k_{mono} than did controls ($P < 0.05$). RV oxidative metabolism was correlated with the mean pulmonary arterial pressure (mPAP) ($r = 0.44$, $P = 0.021$), pulmonary vascular resistance (PVR) ($R = 0.56$, $P = 0.002$), and brain natriuretic peptide (BNP) ($R = 0.42$, $P = 0.029$). Members of the PH therapy group had reduced RV oxidative metabolism ($P = 0.002$) and improved RV work/oxygen consumption index ($P < 0.001$).

Conclusions: RV oxidative metabolism increased as the correlation between mPAP and PVR increased. PH-specific treatments reduced RV oxidative metabolism. Therefore, RV metabolism and its efficiency can provide new pathophysiological insights and will be a new therapeutic marker in patients with PH.

Keywords Metabolism • Pulmonary hypertension • Right ventricle • Tomography

15.1 Introduction

The right ventricle (RV) is the anterior cardiac chamber located just behind the sternum. The RV receives systemic venous return and pumps it into the pulmonary arteries [1]. Under normal conditions, the RV requires little energy to pump venous blood to the pulmonary arteries since pulmonary circulation has a much lower vascular resistance than does systemic circulation [2]. The RV therefore usually has low oxygen consumption.

Until recently, most cardiology research was concerned with left ventricle (LV) physiologies and pathologies. In fact, in the early twentieth century, some groups hypothesized that human circulation could be maintained without RV function [3]. However, cardiovascular surgeons recognized the importance of RV function, and RV dysfunction appeared to be associated with major cardiovascular events in heart failure (HF) [4]. In addition, development of state-of-the-art cardiovascular imaging modalities such as echocardiography, cardiac magnetic resonance (CMR) imaging, and positron emission tomography (PET) have made it possible to noninvasively evaluate the functional and physiological characteristics of RV myocardium [5, 6]. Based on this background, research on the RV has progressed intensively in recent years.

One of the major causes of RV dysfunction is pulmonary hypertension (PH). PH is categorized into five groups as follows: Group 1, pulmonary artery hypertension (PAH); Group 2, PH with LV disease; Group 3, PH associated with lung disease and/or hypoxia; Group 4, PH due to chronic thrombosis and/or embolism; and Group 5, miscellaneous [7]. Elevated pulmonary arterial pressure (PAP) and pulmonary vascular resistance (PVR) may induce RV dysfunction in patients with PH

[7]. However, the RV has a high capacity to adapt to pressure or volume overload before failing in its function [8]. Before myocardial fibrosis and RV heart failure develop, moderate to severe PH often leads to initial RV adaptation [9]. Given the increased arterial pressure in pulmonary circulation, the RV may require a significant power output in response to increased afterload, and this may increase the demand for oxygen in the RV [10]. In this circumstance, the RV may require improved mechanical efficiency in order to increase the power output. A study by Wong et al. showed that idiopathic PH with RV dysfunction was associated with increased RV myocardial oxygen consumption (MVO_2) and reduced RV efficiency [11], a situation possibly mirroring the case of LV energetics in heart failure [12–14]. However, the study by Wong et al. lacked control subjects [11]. Yoshinaga et al. evaluated the RV oxidative metabolism in patients with PH and showed that patients with PH had increased oxidative metabolism in comparison with that of normal individuals [15]. Increasing RV oxidative metabolism was associated with several prognostic markers such as mean PAP (mPAP), PVR, and brain natriuretic peptide (BNP). These findings suggest that elevated RV oxidative metabolism may be a prognostic marker.

^{11}C-acetate PET is a noninvasive technique for measuring regional and global myocardial oxidative metabolism [13, 16–19], which is correlated with tricarboxylic acid cycle flux and MVO_2 [16]. RV myocardial oxidative metabolism can also be measured noninvasively using ^{11}C-acetate PET [15, 17, 20–22]. HF therapies such as beta-blockers that reduce MVO_2 are considered to improve the survival of patients with HF [23]. LV cardiac efficiency can be estimated noninvasively [12] by combining the mechanical work with the oxidative metabolism as measured by ^{11}C-acetate PET. This form of LV efficiency measurement has been applied to evaluate several new HF treatments including beta-blockers, cardiac resynchronized therapy, surgical reconstruction therapy, and obstructive sleep apnea (OSA) syndrome treatments [13, 14, 24–26].

PH-specific vasodilators such as endothelin receptor antagonists, phosphodiesterase-5 inhibitors, and prostacyclin decrease pulmonary arterial pressure [7, 27]. These new vasodilators indeed improve survival in PH patients. Oikawa et al. reported that reducing mPAP through the use of epoprostenol was associated with reduced RV glucose metabolism observed by ^{18}F-fluorodeoxyglucose (FDG) PET [28]. However, it is not clear whether such a treatment favorably affects RV myocardial oxidative metabolism.

The purpose of this study was to investigate the possible impacts of the intensified PH-specific vasodilator therapy on myocardial energetics using ^{11}C-acetate PET.

15.2 Materials and Methods

15.2.1 Study Subjects

Study subjects were recruited from the first department of medicine at the Hokkaido University Hospital. The patient inclusion criteria were as follows: (1) a resting mPAP $\geq$ 25 mmHg and a pulmonary capillary wedge pressure (PCWP) $\leq$

15 mmHg [7], (2) symptoms of PH in accordance with World Health Organization (WHO) functional class II or III, (3) PH subtypes chronic thromboembolic pulmonary hypertension (CTEPH) or PAH [29], and (4) stable condition (unchanged for >4 weeks).

Exclusion criteria were secondary PH due to LV disease, unstable condition of patients, and permanent pacemaker implantation.

The study was approved by the Hokkaido University Graduate School of Medicine Human Research Ethics Board. Written informed consent was obtained from all patients.

15.2.2 Experimental Protocol

14 PH patients underwent right heart catheterization. Precapillary PH was diagnosed based on a mPAP ≥ 25 mmHg at rest and a PCWP ≤ 15 mmHg [7]. Among the 14 PH patients, nine patients started or added the PH-specific vasodilators based on the combined guidelines of the European Society of Cardiology (ESC) and the European Respiratory Society (ERS), and these nine patients were categorized as the intensified treatment group [30]. The remaining five patients did not change their treatments and served as a control group.

Within 7 days of right heart catheterization, all patients underwent blood sampling, CMR, and ^{11}C-acetate PET at rest on the same day [15]. CMR and ^{11}C-acetate PET were repeated after 10.7 ± 6.5 months for the intensified treatment group (Fig. 15.1). Patients with PH but without OSA served as the control group

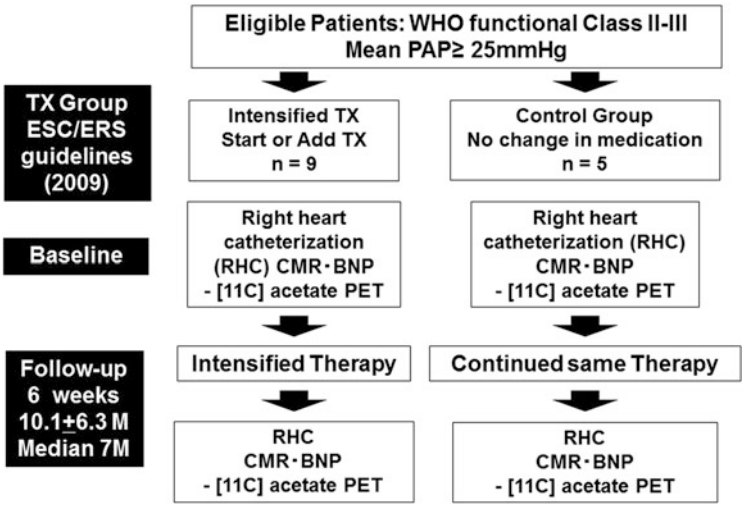

Fig. 15.1 Study design of the current study. *BNP* brain natriuretic peptide, *CMR* cardiac magnetic resonance, *RHC* right heart catheterization, *TX* treatment

and underwent CMR and ^{11}C-acetate PET at rest at baseline and after 10.6 ± 6.3 months ($P = \text{NS}$).

WHO functional class evaluation and blood tests including BNP were measured at baseline and follow-up.

15.2.3 Right Heart Catheterization

A complete hemodynamic evaluation was performed in all PH patients using the standard technique for right heart catheterization. The hemodynamic measurements included mean right atrial pressure, mPAP, and mean PCWP. Cardiac output was determined through thermodilution. PVR was calculated as (mPAP – mean PCWP) divided by cardiac output.

15.2.4 Measurements of BNP

Blood samples were obtained for fasting conditions the morning before the PET studies. BNP data were obtained for all patients. Plasma BNP was measured using immunoradiometric assay [31].

15.2.5 Cardiac Magnetic Resonance Imaging

CMR imaging studies were performed using a 1.5-T Achieva magnetic resonance imaging system (Philips Medical Systems, Best, the Netherlands) equipped with master gradients (maximum gradient amplitude 33 mT/m and maximum slew rate 100 mT/m/msec). CMR data acquisition was performed on patients in the supine position with breath-holding in expiration. We used a five-element cardiac phased-array coil and a vector cardiographic method for electrocardiogram (ECG)-gating images. We performed localizing scans with breath-hold cine imaging and axial orientation. Coronal images were used for cardiac anatomy evaluation. CMR images spanned from bronchial bifurcation to diaphragm level thus allowing for whole-heart analysis. We obtained 12 short-axis cine slices during a steady-state free precession pulse sequence. The precession pulse sequence was as follows: repetition time = 2.8 msec, echo time = 1.4 msec, flip angle = 60, acquisition matrix = 192×256, field of view = 380 mm, slice thickness = 10 mm, inter-slice gap = 0 mm, and phases/cardiac cycle = 20 [32].

15.2.6 CMR Data Analysis

CMR images were analyzed using commercially available software (Extended MR Work Space: version 2.6.3, Philips Medical Systems, Amsterdam, the Netherlands). RV and LV volumes were measured using cine long-axis images. RV and LV endocardial borders were semiautomatically traced. We then calculated the RV ejection fraction (EF), LVEF, and RV volumes using this information [15]. RVEF was measured in transverse (axial) orientation. LVEF was measured in short-axial orientation [33]. All CMR images were analyzed by clinicians blinded to the clinical and imaging data.

15.2.7 Positron Emission Tomography

All patients were instructed to fast overnight. PH patients who had vasodilator treatments took their morning medications before the PET and CMR studies. Patients were positioned with the heart centered in the field of view in a whole-body PET scanner (ECAT HR+, Siemens/CTI Knoxville, TN) [34]. Dynamic PET acquisition was initiated (10×10 s (s); 2×30s; 5×100 s; 3×180 s; 2×300 s) [14] followed by intravenous administration of 20 mCi (mCi) [740 megabecquerel (MBq)] ^{11}C-acetate.

15.2.8 ^{11}C-Acetate PET Data Analysis

The reconstructed dynamic PET images were analyzed by applying a region of interest over the whole LV and free wall of the RV myocardium in 3–5 mid-ventricular transaxial planes [15, 20, 26]. A mono-exponential function was fit to the myocardial time-activity data. The clearance rate constant (k_{mono}) was determined as described previously [13, 14, 34]. The mono-exponential fit began at the point when the blood pool was stable (usually 2–4 min after injection) (Fig. 15.2).

All data were analyzed by clinicians blinded to the clinical and imaging data.

15.2.9 RV Work Per MVO_2 Index Calculation

The ^{11}C-acetate clearance data were combined with the stroke work data to derive myocardial efficiency using the LV work metabolic index (WMI) using the following equation [13, 14, 26].

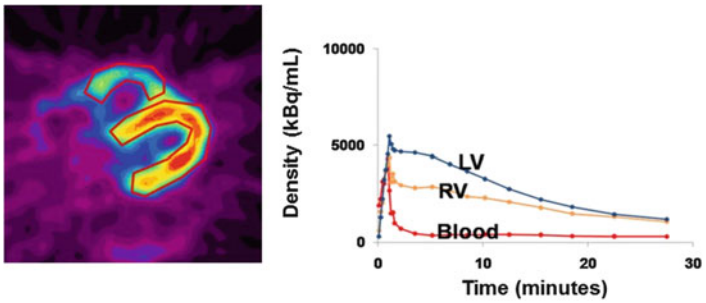

Fig. 15.2 Example of left and right myocardial time-activity data from a ^{11}C-acetate PET acquisition. A mono-exponential function fit to the myocardial clearance yields a clearance rate constant; k_{mono} represents the rate of oxidative metabolism and reflects MVO_2. Blue line represents left ventricular (LV) myocardium time-activity curve. Orange line represents right ventricular (RV) myocardium time-activity curve. Red line indicates blood time-activity curve

$WMI = SVI \times SBP \times HR/k_{mono}$; where SVI is the stroke volume index determined by CMR, SBP is systolic blood pressure, HR is heart rate, and k_{mono} is the mono-exponential rate constant for ^{11}C-acetate clearance from the myocardium.

As a modified LV work metabolic index equation, the RV work per MVO_2 index was calculated as the ratio of RV SVI measured by CMR divided by RV MVO_2. The equation was as follows [35]:

$$\text{RV work per MVO}_2\text{index} \;=\; \text{RV SVI} \,/\, \text{RV } k_{mono} \times \text{RV mass} \;\times\; 20$$

15.2.10 Statistical Analysis

Continuous variables (using a logarithmic transformation on skewed distributions as appropriate) are presented as mean and standard deviations. Categorical variables are presented as frequencies with percentages. Differences in results for the PH group and the control group were examined for statistical significance with a two-sample *t*-test for continuous variables. A *P* value of less than 0.05 was considered indicative of a statistically significant difference. Statistical calculations were carried out using SAS software version 9.2 (SAS Institute, Inc., Cary, NC).

15.3 Results

15.3.1 Patient Characteristics

A total of 14 WHO functional class II or III PH patients were prospectively enrolled in the study between December 2009 and July 2011, and all PH patients completed the study protocol.

Table 15.1 Patient characteristics

	Intensified treatment ($n = 9$)	Control ($n = 5$)	*P* value intensified treatment vs. control
Characteristics			
Age (y)	48.4 ± 12.9	52.8 ± 17.5	NS
Male/female	3/6	2/3	NS
Medications			
Vasodilators			
No vasodilators	1	5	
Hemodynamics	8	0	
Right heart catheterization			
Systolic PAP (mmHg)	60.9 ± 19.5	53.2 ± 8.8	0.14
Diastolic PAP (mmHg)	24.8 ± 6.4	19.4 ± 8.0	0.54
Mean PAP (mmHg)	37.8 ± 9.2	32.6 ± 7.4	0.7
PVR (dynes $+s^{-1}+cm^{-5}$)	564.4 ± 246.93	514.6 ± 149.4	0.35

Values are mean ± SD when appropriate
PAP pulmonary arterial pressure, *PVR* pulmonary vascular resistance

The baseline characteristics of the participants are shown in Table 15.1. There was no significant difference in mean age between members of the intensified PH treatment patient group and those of the control group.

15.3.2 Right Heart Catheterization

The baseline right heart catheterization data is shown in Table 15.1. There was no significant difference in the systolic PAP, diastolic PAP, mPAP, and PVR of the intensified PH treatment group and those of the control group.

15.3.3 LV and RV Systolic Function

The RVEF and LVEF were similar in both the intensified PH treatment group and the control group (Table 15.2).

Table 15.2 LV and RV functional measurements

	Intensified treatment ($n = 9$)	Control ($n = 5$)	P value intensified treatment vs. control
LVEF (%)	57.5 ± 10.5	61.0 ± 7.3	0.50
RVEF (%)	32.1 ± 13.0	34.7 ± 9.7	0.59
LV k_{mono} (min^{-1})	0.052 ± 0.008	0.058 ± 0.006	0.72
RV k_{mono} (min^{-1})	0.043 ± 0.008	0.044 ± 0.01	0.18
SVI/RV k_{mono} ($mL/min^{-1} \cdot m^2$)	730.8 ± 253.6	829.1 ± 362.9	0.31

Values are mean ± SD when appropriate
LV left ventricular, *LVEF* left ventricular ejection fraction, *RV* right ventricular, *RVEF* right ventricular ejection fraction, *RVSV* right ventricular stroke volume

15.3.4 LV and RV Oxidative Metabolism

There was no statistically significant difference between the LV oxidative metabolism, k_{mono}, of the intensified PH treatment group and that of the controls ($P = 0.72$). There was also no statistically significant difference between the RV oxidative metabolism, k_{mono}, of the intensified PH treatment group and that of the controls ($P = 0.18$) (Table 15.2). In addition, the RV SVI per RV k_{mono} was similar in both the intensified PH treatment group and the control group ($P = 0.31$).

15.3.5 Longer-Term Effects of Intensified PH-Specific Therapy on RV Metabolism and Work per Oxygen Consumption

The intensified PH therapy group tended to have reduced PVR compared with that of the control group (−20.6 ± 41.7 vs. −3.4 ± 33.2 %, $P = 0.29$). Intensified PH therapy tended to reduce BNP (377.2 ± 694.5 to 70.8 ± 132.6 mol/mL, $P = 0.18$).

Intensified PH therapy significantly reduced RV oxidative metabolism (0.044 ± 0.008 to 0.039 ± 0.007/min, $P = 0.002$) while increasing SVI (31.4 ± 10.1 to 39.3 ± 9.6 mL/m^2, $P = 0.017$) (Fig. 15.3). As a result, the intensified PH-specific therapy significantly improved the RV work/oxygen consumption index (730.8 ± 253.6 to 1038.5 ± 262.7 $mL/min + m^2$, $P < 0.001$) (Fig. 15.4). There was no significant change in LV k_{mono} in this group (0.052 ± 0.008 to 0.050 ± 0.006/min, $P = 0.35$). The control group showed no changes in these parameters (RV k_{mono}: 0.041 ± 0.006 to 0.049 ± 0.01/min, $P = 0.15$, RV work/oxygen consumption index: 829.1 ± 362.9 to 721.5 ± 241.2 $mL/min + m^2$, $P = 0.69$).

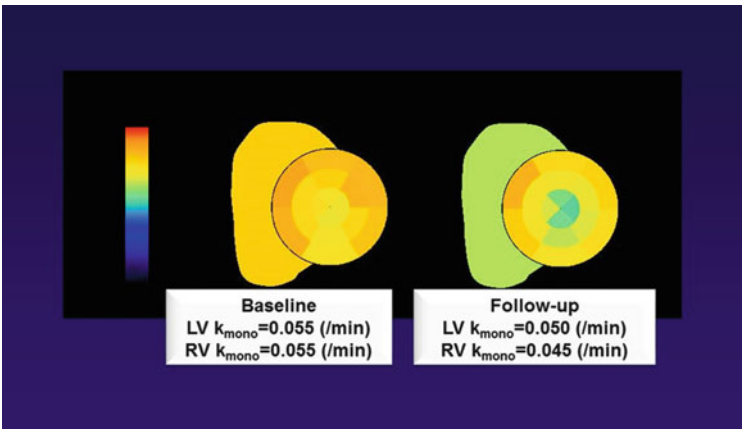

Fig. 15.3 Representative case of PAH patient who had intensified PH-specific vasodilator therapy. LV k_{mono} did not change after the intensified PH-specific vasodilator treatment. In contrast, RV k_{mono} was markedly reduced after the intensified PH-specific vasodilator therapy

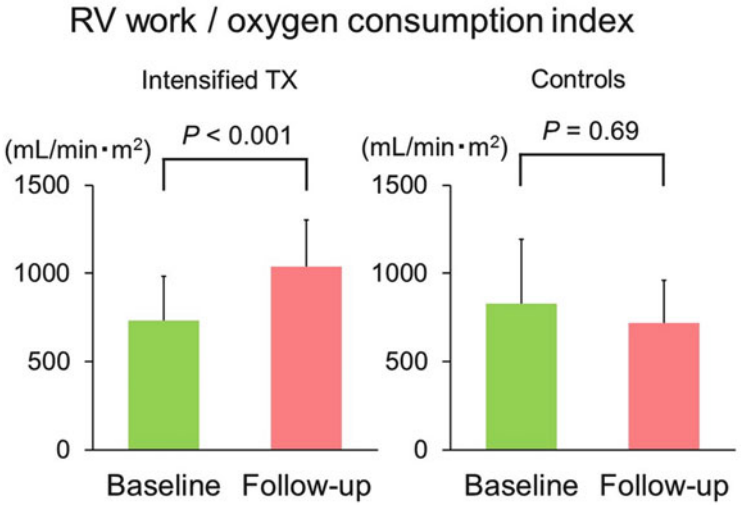

Fig. 15.4 Effects of intensified PH-specific vasodilator therapy on RV work per oxygen consumption index. Patients who had intensified PH-specific vasodilator therapy had a significantly improved RV work per oxygen consumption index. In contrast, there was no significant difference in RV work per oxygen consumption index in control group. *PH* pulmonary hypertension, *RV* right ventricle, *TX* therapy

15.4 Discussion

Intensified PH-specific vasodilator therapy tended to reduce PVR and BNP. The intensive PH-specific therapy led to reduction in right ventricular oxidative metabolism and a significant improvement in right ventricular work per oxygen consumption index in patients with pulmonary hypertension.

15.4.1 Increased RV Oxidative Metabolism in Patients with PH

The major determinants of myocardial metabolism are heart rate, contractility, and wall stress [36, 37]. Oxygen demand in the RV may also increase with elevated PAP [10].

In LV, heart failure is considered to be an energy-depleted state. Improved survival through the use of beta-blockers and vasodilator therapy is in part associated with the energy-sparing effects of these medications [38].

RV MVO_2 was originally measured through right coronary venous blood sampling [10]. As noninvasive approaches, ^{11}C-acetate and ^{15}O-labeled tracers PET have also been applied for RV oxidative measurements in HF and PH [15, 17, 22, 26, 39, 40]. The current data revealed increased RV oxidative metabolism in patients with PH and reduced RV contraction. The current data agreed with findings of our previous study and the study by Wong et al. [15, 39].

15.4.2 Study Population and Effects of PH-Specific Vasodilator Therapy

In the current study, eight PH patients did not have PH-specific vasodilator therapy. One patient had a PH-specific vasodilator, but the PH control did not reach the standard control level. Therefore, these nine patients either started or added the PH-specific vasodilator. The remaining five patients already received PH-specific vasodilator treatments and they were stable. These five patients did not meet the criteria to add further vasodilators to control their PH based on ESC and ERS guidelines [30].

The intensified PH therapy group tended to have reduced mPAP. Although the mPAP did not reach statistically significant levels, this finding may be due to the small sample size, but it may still indicate that intensified PH-specific therapy had beneficial effects. In fact, BNP also tended to be reduced after the therapy, a finding that may indicate a secondary reduction in wall stress due to reduced mPAP. It may therefore be appropriate to evaluate the therapeutic effects on RV energetics in this study population.

15.4.3 Effects of PH-Specific Vasodilator Therapy on RV Oxidative Metabolism and Work per MVO_2 Index

In the previous study, we evaluated RV power and RV efficiency using the following equation: RV efficiency = HR × mPAP × SV × 1.33×10^{-4}/RV k_{mono} × RV mass × 20 [35]. Using this equation, WHO functional classification II and III PH patients actually had increased RV power and RV efficiency compared to patients in the control group [15]. The increasing power and RV efficiency may be adaptive processes associated with increasing mPAP. In the LV, the LV efficiency is estimated using the WMI. The WMI was calculated as follows: WMI = SVI × SBP × HR/k_{mono} [13]. LVHF treatments usually do not significantly change the HR and SBP [14]. In contrast, PH-specific vasodilators significantly reduce the mPAP [27]. Therefore, if the equation proposed by Sun et al. is simply applied to RV efficiency measurements [35], RV efficiency may be reduced after PH-specific vasodilator therapy since the reduction of mPAP would play a significant role over the increasing SVI. The afterload of pulmonary circulation is usually lower than that of systemic circulation [1, 41]. Therefore, the RV may have volume efficiency rather than pressure efficiency as would apply in the case of the LV. Therefore, we applied SVI per MVO_2 index instead of Sun's equation in the current study.

The SVI per MVO_2 index shows that the intensified PH-specific vasodilator therapy significantly improved this parameter in comparison with that of controls. The trend of mPAP reduction may contribute to these improvements. Therefore, improving volume efficiency in the RV may be one of the therapeutic effects of PH-specific vasodilators, and doing so may contribute to the improvement of outcomes in patients with PH. This hypothesis should be tested in a larger study population in the future.

15.4.4 Limitations

The thickness of the RV free wall is usually 4–5 mm, which is thinner than the LV free wall. However, the current study population had thicker RV walls. When radiotracer uptake is measured, the partial volume effect may significantly attenuate the data. However, we analyzed the oxidative metabolism using mono-exponential fitting. This approach measures clearance of the radiotracer from the myocardium. Thus, the partial volume effect should be minimal.

15.5 Conclusion

Intensified PH-specific vasodilator therapy led to a reduction in right ventricular oxidative metabolism and a significant improvement in right ventricular work per oxygen consumption index in patients with pulmonary hypertension. These effects may contribute to the benefits of intensified PH-specific vasodilator therapy.

Conflicts of Interest None

Acknowledgments The authors thank Keiichi Magota, PhD; Ken-ichi Nishijima, PhD; Daisuke Abo, MSc; and Eriko Suzuki for their support for this study. This manuscript has been reviewed by a North American English-language professional editor, Ms. Holly Beanlands. The authors also thank Ms. Holly Beanlands for critical reading of the manuscript.

This study was supported in part by grants from the Japanese Ministry of Education, Culture, Sports, Science and Technology (Category B, No. 23390294), Hokkaido Heart Association (H-20) (Sapporo, Japan), Adult Vascular Disease Research Foundation (#H22-23) (Kyoto, Japan), North-Tech Research Foundation (#H23-S2-17, Sapporo, Japan), and grants from the Innovation Program of the Japan Science and Technology Agency. Dr. Yoshinaga is supported by the Imura Clinical Research Award (Adult Vascular Disease Research Foundation).

References

1. Haddad F, Hunt SA, Rosenthal DN, Murphy DJ. Right ventricular function in cardiovascular disease, part I: Anatomy, physiology, aging, and functional assessment of the right ventricle. Circulation. 2008;117:1436–48. doi:10.1161/CIRCULATIONAHA.107.653576.
2. Dell'Italia LJ. The right ventricle: anatomy, physiology, and clinical importance. Curr Probl Cardiol. 1991;16:653–720.
3. Lee FA. Hemodynamics of the right ventricle in normal and disease states. Cardiol Clin. 1992; 10:59–67.
4. Meyer P, Filippatos GS, Ahmed MI, Iskandrian AE, Bittner V, Perry GJ, et al. Effects of right ventricular ejection fraction on outcomes in chronic systolic heart failure. Circulation. 2010;121:252–8. doi:10.1161/CIRCULATIONAHA.109.887570.
5. Champion HC, Michelakis ED, Hassoun PM. Comprehensive invasive and noninvasive approach to the right ventricle-pulmonary circulation unit: state of the art and clinical and research implications. Circulation. 2009;120:992–1007. doi:10.1161/CIRCULATIONAHA.106.674028.
6. Valsangiacomo Buechel ER, Mertens LL. Imaging the right heart: the use of integrated multimodality imaging. Eur Heart J. 2012;33:949–60. doi:10.1093/eurheartj/ehr490.

7. Chin KM, Rubin LJ. Pulmonary arterial hypertension. J Am Coll Cardiol. 2008;51:1527–38.
8. Haddad F, Doyle R, Murphy DJ, Hunt SA. Right ventricular function in cardiovascular disease, part II: pathophysiology, clinical importance, and management of right ventricular failure. Circulation. 2008;117:1717–31. doi:10.1161/CIRCULATIONAHA.107.653584.
9. Chin KM, Kim NH, Rubin LJ. The right ventricle in pulmonary hypertension. Coron Artery Dis. 2005;16:13–8.
10. Zong P, Tune JD, Downey HF. Mechanisms of oxygen demand/supply balance in the right ventricle. Exp Biol Med (Maywood). 2005;230:507–19.
11. Wong YY, Ruiter G, Lubberink M, Raijmakers PG, Knaapen P, Marcus JT, et al. Right ventricular failure in idiopathic pulmonary arterial hypertension is associated with inefficient myocardial oxygen utilization. Circ Heart Fail. 2011;4:700–6. doi:10.1161/CIRCHEARTFAILURE.111.962381.
12. Ukkonen H, Beanlands R. Oxidative metabolism and cardiac efficiency. In: Wahl R, editor. Principles and practice of PET and PET/CT. 2nd ed. Philadelphia: Lippincott Williams & Wilkins; 2009. p. 589–606.
13. Beanlands RS. Nahmias C, Gordon E, Coates G, deKemp R, Firnau G, et al. The effects of beta(1)-blockade on oxidative metabolism and the metabolic cost of ventricular work in patients with left ventricular dysfunction: A double-blind, placebo-controlled, positron-emission tomography study. Circulation. 2000;102:2070–5.
14. Yoshinaga K, Burwash IG, Leech JA, Haddad H, Johnson CB. deKemp RA, et al. The effects of continuous positive airway pressure on myocardial energetics in patients with heart failure and obstructive sleep apnea. J Am Coll Cardiol. 2007;49:450–8.
15. Yoshinaga K, Ohira H, Tsujino I, Oyama-Manabe N, Mielniczuk L, Beanlands RS, et al. Attenuated right ventricular energetics evaluated using (1)(1)C-acetate PET in patients with pulmonary hypertension. Eur J Nucl Med Mol Imaging. 2014;41:1240–50. doi:10.1007/s00259-014-2736-4.
16. Armbrecht JJ, Buxton DB, Brunken RC, Phelps ME, Schelbert HR. Regional myocardial oxygen consumption determined noninvasively in humans with [1-11C]acetate and dynamic positron tomography. Circulation. 1989;80:863–72.
17. Stolen KQ, Kemppainen J, Ukkonen H, Kalliokoski KK, Luotolahti M, Lehikoinen P, et al. Exercise training improves biventricular oxidative metabolism and left ventricular efficiency in patients with dilated cardiomyopathy. J Am Coll Cardiol. 2003;41:460–7.
18. Yoshinaga K, Chow BJ, Dekemp RA, Thorn S, Ruddy TD, Davies RA, et al. Application of cardiac molecular imaging using positron emission tomography in evaluation of drug and therapeutics for cardiovascular disorders. Curr Pharm Des. 2005;11:903–32.
19. Yoshinaga K, Tamaki N. Imaging myocardial metabolism. Curr Opin Biotechnol. 2007;18:52–9. doi:10.1016/j.copbio.2006.11.003.
20. Ukkonen H, Saraste M, Akkila J, Knuuti J, Karanko M, Iida H, et al. Myocardial efficiency during levosimendan infusion in congestive heart failure. Clin Pharmacol Ther. 2000;68:522–31.
21. Wong YY, Raijmakers P, van Campen J, van der Laarse WJ, Knaapen P, Lubberink M, et al. 11C-Acetate clearance as an index of oxygen consumption of the right myocardium in idiopathic pulmonary arterial hypertension: a validation study using 15O-labeled tracers and PET. J Nucl Med. 2013;54:1258–62. doi:10.2967/jnumed.112.115915.
22. Ohira H, Beanlands RS, Davies RA, Mielniczuk L. The role of nuclear imaging in pulmonary hypertension. J Nucl Cardiol. 2015;22:141–57. doi:10.1007/s12350-014-9960-y.
23. Packer M, Bristow MR, Cohn JN, Colucci WS, Fowler MB, Gilbert EM, et al. The effect of carvedilol on morbidity and mortality in patients with chronic heart failure. U.S. Carvedilol Heart Failure Study Group. N Engl J Med. 1996;334:1349–55. doi:10.1056/NEJM199605233342101.
24. Chiba S, Naya M, Iwano H, Yoshinaga K, Katoh C, Manabe O, et al. Interrelation between myocardial oxidative metabolism and diastolic function in patients undergoing surgical ventricular reconstruction. Eur J Nucl Med Mol Imaging. 2013;40:349–55. doi:10.1007/s00259-012-2297-3.

25. Hall AB, Ziadi MC, Leech JA, Chen SY, Burwash IG, Renaud J, et al. Effects of short-term continuous positive airway pressure on myocardial sympathetic nerve function and energetics in patients with heart failure and obstructive sleep apnea: a randomized study. Circulation. 2014;130:892–901. doi:10.1161/CIRCULATIONAHA.113.005893.
26. Ukkonen H, Beanlands RS, Burwash IG, de Kemp RA, Nahmias C, Fallen E, et al. Effect of cardiac resynchronization on myocardial efficiency and regional oxidative metabolism. Circulation. 2003;107:28–31.
27. Galie N, Corris PA, Frost A, Girgis RE, Granton J, Jing ZC, et al. Updated treatment algorithm of pulmonary arterial hypertension. J Am Coll Cardiol. 2013;62:D60–72. doi:10.1016/j.jacc.2013.10.031.
28. Oikawa M, Kagaya Y, Otani H, Sakuma M, Demachi J, Suzuki J, et al. Increased [18F] fluorodeoxyglucose accumulation in right ventricular free wall in patients with pulmonary hypertension and the effect of epoprostenol. J Am Coll Cardiol. 2005;45:1849–55.
29. Simonneau G, Robbins IM, Beghetti M, Channick RN, Delcroix M, Denton CP, et al. Updated clinical classification of pulmonary hypertension. J Am Coll Cardiol. 2009;54:S43–54. doi:10.1016/j.jacc.2009.04.012.
30. Task Force for D, Treatment of Pulmonary Hypertension of European Society of C, European Respiratory S, International Society of H, Lung T, Galie N, et al. Guidelines for the diagnosis and treatment of pulmonary hypertension. Eur Respir J. 2009;34:1219–63. doi:10.1183/09031936.00139009.
31. Nagaya N, Nishikimi T, Uematsu M, Satoh T, Kyotani S, Sakamaki F, et al. Plasma brain natriuretic peptide as a prognostic indicator in patients with primary pulmonary hypertension. Circulation. 2000;102:865–70.
32. Alfakih K, Plein S, Bloomer T, Jones T, Ridgway J, Sivananthan M. Comparison of right ventricular volume measurements between axial and short axis orientation using steady-state free precession magnetic resonance imaging. J Magn Reson Imaging. 2003;18:25–32. doi:10.1002/jmri.10329.
33. Oyama-Manabe N, Sato T, Tsujino I, Kudo K, Manabe O, Kato F, et al. The strain-encoded (SENC) MR imaging for detection of global right ventricular dysfunction in pulmonary hypertension. Int J Cardiovasc Imaging. 2013;29:371–8. doi:10.1007/s10554-012-0105-6.
34. Yoshinaga K, Katoh C, Beanlands RS, Noriyasu K, Komuro K, Yamada S, et al. Reduced oxidative metabolic response in dysfunctional myocardium with preserved glucose metabolism but with impaired contractile reserve. J Nucl Med. 2004;45:1885–91.
35. Sun KT, Yeatman LA, Buxton DB, Chen K, Johnson JA, Huang SC, et al. Simultaneous measurement of myocardial oxygen consumption and blood flow using [1-carbon-11]acetate. J Nucl Med. 1998;39:272–80.
36. Braunwald E. Control of myocardial oxygen consumption: physiologic and clinical considerations. Am J Cardiol. 1971;27:416–32.
37. Laine H, Katoh C, Luotolahti M, Yki-Jarvinen H, Kantola I, Jula A, et al. Myocardial oxygen consumption is unchanged but efficiency is reduced in patients with essential hypertension and left ventricular hypertrophy. Circulation. 1999;100:2425–30.
38. Katz AM. Potential deleterious effects of inotropic agents in the therapy of chronic heart failure. Circulation. 1986;73:III184–90.
39. Wong YY, Westerhof N, Ruiter G, Lubberink M, Raijmakers P, Knaapen P, et al. Systolic pulmonary artery pressure and heart rate are main determinants of oxygen consumption in the right ventricular myocardium of patients with idiopathic pulmonary arterial hypertension. Eur J Heart Fail. 2011;13:1290–5. doi:10.1093/eurjhf/hfr140.
40. Knaapen P, Germans T, Knuuti J, Paulus WJ, Dijkmans PA, Allaart CP, et al. Myocardial energetics and efficiency: current status of the noninvasive approach. Circulation. 2007;115:918–27. doi:10.1161/CIRCULATIONAHA.106.660639.
41. Sheehan F, Redington A. The right ventricle: anatomy, physiology and clinical imaging. Heart. 2008;94:1510–5. doi:10.1136/hrt.2007.132779.

Chapter 16
Usefulness of ^{18}F-FDG PET in Diagnosing Cardiac Sarcoidosis

Osamu Manabe, Keiichiro Yoshinaga, Hiroshi Ohira, and Noriko Oyama-Manabe

Abstract Sarcoidosis is a multisystem granulomatous disorder of unknown etiology. The number of patients with cardiac involvement is considered to be limited, but cardiac sarcoidosis is a very serious and unpredictable aspect of sarcoidosis resulting in conduction-system abnormalities and heart failure. The severity of cardiac involvement depends on the extent and location of the granulomatous lesions.

When establishing a diagnosis, ^{18}F-fluorodeoxyglucose (^{18}F-FDG) positron emission tomography (PET) is a useful tool to detect active inflammatory lesions associated with sarcoidosis. The heart uses different energy sources including free fatty acids (FFA), glucose, and others. The ^{18}F-FDG is an analog of glucose, and for the precise evaluation of the extent and severity of cardiac involvement, recent studies have focused on reducing physiological myocardial ^{18}F-FDG uptake. Long fasting and dietary modification, such as observing a low-carbohydrate or high-fat diet, are the recommended regimens for preparations to make a precise evaluation. The FFA level before the PET scan could be a predictor of the success to the suppression of the physiological ^{18}F-FDG accumulation.

With ^{18}F-FDG PET therapy monitoring or risk stratification based on quantitative ^{18}F-FDG accumulation becomes possible. The quantification of the volume and intensity of ^{18}F-FDG uptake could assist in predicting the clinical outcomes and in evaluating the efficiency of steroid treatments.

O. Manabe (✉)
Department of Nuclear Medicine, Hokkaido University Graduate School of Medicine, Sapporo, Japan
e-mail: osamumanabe817@med.hokudai.ac.jp

K. Yoshinaga
Department of Nuclear Medicine, Hokkaido University Graduate School of Medicine, Kita15 Nishi7, Kita-Ku, Sapporo 060-8638, Hokkaido, Japan

Molecular Imaging Research Center, National Institute of Radiological Sciences, 4-9-1 Anagawa, Inage-Ku, Chiba 263-8555, Japan

H. Ohira
First Department of Medicine, Hokkaido University Hospital, Sapporo, Japan

N. Oyama-Manabe
Diagnostic and Interventional Radiology, Hokkaido University Hospital, Sapporo, Japan

Y. Kuge et al. (eds.), *Perspectives on Nuclear Medicine for Molecular Diagnosis and Integrated Therapy*, DOI 10.1007/978-4-431-55894-1_16

This report provides a summary of the usefulness of ^{18}F-FDG PET in its current status as a diagnostic modality for cardiac sarcoidosis.

Keywords Cardiac sarcoidosis • Positron emission tomography • Fluorodeoxyglucose

16.1 Background

Sarcoidosis is a multisystem granulomatous disorder of unknown etiology. It is characterized by noncaseating, epithelioid granulomas. Typically, young or middle-aged adults are affected. In Japan, the annual incidence ranges from 1 to 2 cases per 100,000 of the population. The bilateral hilar and mediastinal lymph nodes, lungs, skin, musculoskeletal system, and eyes are well known to be involved in lesions. Essentially all organs, including the heart, may potentially be involved [1, 2].

Sarcoidosis patient treatment generally follows a favorable clinical course. However, about 30 % of patients suffer chronically or experience recurrence. Granulomas forming in an organ can affect how the organ functions and be a cause of signs and symptoms. Especially, prognosis is related to the presence of cardiac lesions [3].

The frequency of cardiac involvement varies and is significantly influenced by ancetstry. In Japan over 25 % of cases with sarcoidosis experience symptomatic cardiac involvement, whereas in the USA and Europe, only about 5 % of cases present cardiac involvement. Autopsy studies in the USA have shown the frequency of cardiac involvement to be about 20 %, whereas autopsy studies in Japan have shown a frequency above 50 % [4–6].

16.2 Diagnostic Criteria for Cardiac Sarcoidosis

Histologic analysis of operative or endomyocardial biopsy specimens could be the irrefutably best standard in diagnosing cardiac sarcoidosis. However, it is not feasible to perform endomyocardial biopsies on all suspected regions, and myocardial biopsies tend to have lower sensitivity in the diagnosis of cardiac sarcoidosis. Therefore, the Japanese Ministry of Health and Welfare (JMHW) guidelines for diagnostic imaging have been used as the diagnostic standard since early times [7]. The JMHW criteria include both the histologic and the clinical diagnosis groups. For the clinical diagnosis group, the positive findings of electrocardiography, echocardiography, and ^{67}Ga scintigraphy are the major criteria; minor criteria include findings of electrocardiography, echocardiography, perfusion images, and cardiac magnetic resonance images. Among the criteria, ^{18}F-fluorodeoxyglucose (^{18}F-FDG) positron emission tomography (PET) is not included in the 2006 criteria; it is only noted as a comment that abnormal ^{18}F-FDG accumulation in the heart is a diagnostically useful finding. However, the usefulness of ^{18}F-FDG PET has been increasingly recognized; the Japanese health insurance system

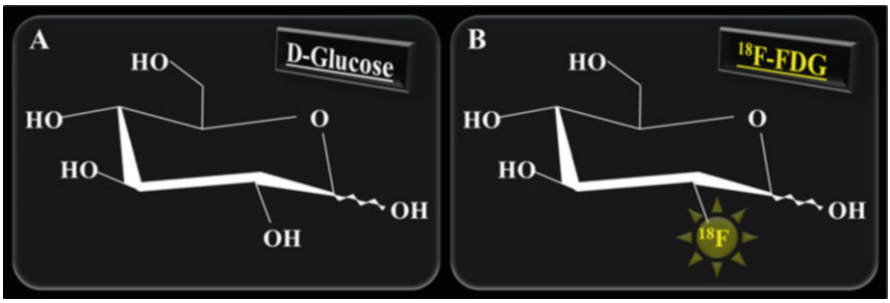

Fig. 16.1 Chemical structural formula of D-glucose and ^{18}F-FDG.
The chemical structural formulas of the glucose and ^{18}F-fluorodeoxyglucose (^{18}F-FDG) are shown in panels A and B, respectively. ^{18}F-FDG is a glucose analog widely used in PET studies of glucose metabolism. ^{18}F-FDG is taken up by plasma-membrane transporters and phosphorylated by the intracellular enzymes in the same manner as glucose. The metabolism of ^{18}F-FDG stops after 6-phosphorylation which is different from glucose and provides an advantage in metabolism studies

approved it for detection of inflammation sites in cardiac sarcoidosis on April 2012. Recently, the Heart Rhythm Society of the USA also proposed the diagnosis and management of cardiac sarcoidosis with ^{18}F-FDG PET and MRI recommended for the evaluation of cardiac sarcoidosis, if there is a cardiac history and abnormality in the electrocardiogram or echocardiography in sarcoidosis patients [8].

16.3 Cardiac Metabolism

For the cardiac metabolism, under long fasting conditions, glucose production and glucose oxidation would decrease. As a result, free fatty acid (FFA) is mobilized from adipose tissue, and the increase in available FFA becomes an alternative source of energy in the myocardium. The ^{18}F-FDG is a glucose analog used clinically in PET to indicate glucose utilization (Fig. 16.1), and physiological myocardial uptake has been reported. The levels of the cardiac uptake vary regardless of blood glucose levels [9].

16.4 ^{18}F-FDG Uptake Patterns in Evaluations of Cardiac Sarcoidosis

To evaluate cardiac sarcoidosis, uptake patterns of ^{18}F-FDG were divided into four kinds as suggested in Fig. 16.2 [7]. Without myocardial ^{18}F-FDG uptake is considered to be negative in active cardiac lesions. A distinct diffuse ^{18}F-FDG uptake in the entire left ventricular wall without localized high ^{18}F-FDG uptake generally is

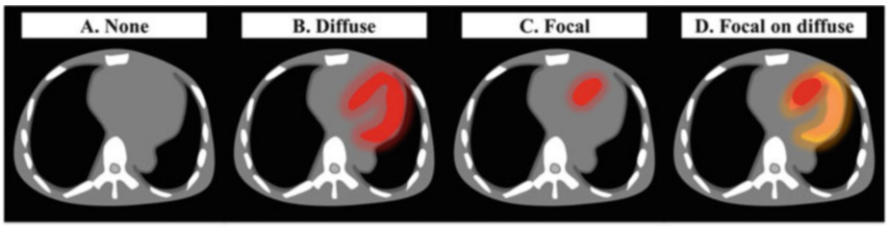

Fig. 16.2 ^{18}F-FDG uptake patterns to evaluate cardiac sarcoidosis.
Uptake patterns were divided into four groups. No ^{18}F-fluorodeoxyglucose (^{18}F-FDG) uptake is considered to be a negative sign for any active cardiac lesion (**a**). A diffuse ^{18}F-FDG uptake in the entire left ventricular wall without any localized high ^{18}F-FDG uptake is generally thought to be a physiological uptake (**b**). With slight accumulation in (**b**), it was not possible to determine if this was caused by cardiac sarcoidosis. Focal uptake (**c**) and focal on diffuse uptakes (**d**) of ^{18}F-FDG in the left ventricular wall are considered to be positive signs for cardiac sarcoidosis

thought to represent a physiological uptake, not indicating an abnormality. Focal and focal on diffuse ^{18}F-FDG uptakes in the left ventricular wall are considered to be positive indicators of cardiac sarcoidosis.

16.5 Preparation for the ^{18}F-FDG PET to Evaluate Cardiac Lesions

The physiological myocardial ^{18}F-FDG uptake may mislead when attempting to establish cardiac sarcoidosis. Proper preparation such as extended fasting with a low-carbohydrate diet before the scan is needed to suppress the physiological cardiac uptake [10]. We have confirmed the usefulness of the effect of 18 h of fasting with a low-carbohydrate diet compared to a minimum 6-h fasting preparation [9]. Patients with at least 6 h of fasting showed a higher diffuse left ventricular (LV) ^{18}F-FDG uptake than patients with longer fasting and low-carbohydrate diets. Patients who fasted for longer and observed a low-carbohydrate diet showed higher FFA levels than a shorter fasting group. In the shorter fasting group, patients with diffuse LV ^{18}F-FDG uptake showed significantly lower FFA levels than patients without a diffuse LV uptake. This shows that the FFA level is an important marker to suppress physiological ^{18}F-FDG uptake. The protocol to obtain better ^{18}F-FDG PET images in cardiac sarcoidosis patients is shown in Fig. 16.3.

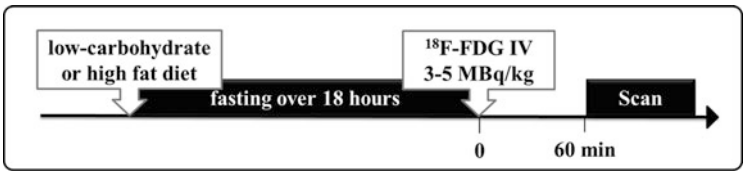

Fig. 16.3 The protocol for the ^{18}F-FDG PET scanning for cardiac sarcoidosis.
Patients were instructed to observe a low-carbohydrate or high-fat diet on the day prior to the scanning, with additional fasting for more than 18 h. The PET images were acquired 60 min after injection of the ^{18}F-FDG

16.6 Location of the ^{18}F-FDG Uptake

Cardiac sarcoidosis provoked the conduction disturbance such as atrioventricular block. There is a relationship between electrocardiogram abnormalities and myocardial ^{18}F-FDG uptake. In particular, the focal ^{18}F-FDG uptake in the interventricular septum in cardiac sarcoidosis is associated with atrioventricular blockage. Therefore, to identify the location of the ^{18}F-FDG uptake is an important issue of potentially great benefit in treatment planning [11].

The ^{18}F-FDG uptake due to inflammation in the LV wall is sometimes difficult to distinguish from the physiological uptake. On the other hand, the physiological uptake in the right ventricle (RV) is less common and less intense. Therefore, although less frequent of the sarcoidosis involvement, the ^{18}F-FDG uptake in the RV due to cardiac sarcoidosis may be useful in diagnosing in sarcoidosis [12].

16.7 Relationship Between ^{18}F-FDG Accumulation and Activity of Sarcoidosis

The significant ^{18}F-FDG accumulation in cardiac sarcoidosis is caused by active inflammatory changes involving activated inflammatory cells like neutrophils, macrophages, and lymphocytes [13], and the ^{18}F-FDG uptake may reflect an active inflammation condition. This makes ^{18}F-FDG PET useful both for the detection of cardiac sarcoidosis as well as for monitoring the treatment response and early recurrence [14].

The maximum standardized uptake value (SUVmax) has been used for semi-quantitative measurements to assess the intensity of ^{18}F-FDG uptake. Recently, the availability of volume-based analysis, such as metabolic volume and total lesion glycolysis, has been widely used to evaluate the extent and activity of the ^{18}F-FDG uptake in malignant tumors [15]. Ahmadian et al. applied volume-based analysis to cardiac sarcoidosis and reported that the metabolic activity estimated by ^{18}F-FDG PET was a reliable independent predictor of cardiac events in cardiac sarcoidosis patients [16]. A volume-based quantification of ^{18}F-FDG uptake could be of value

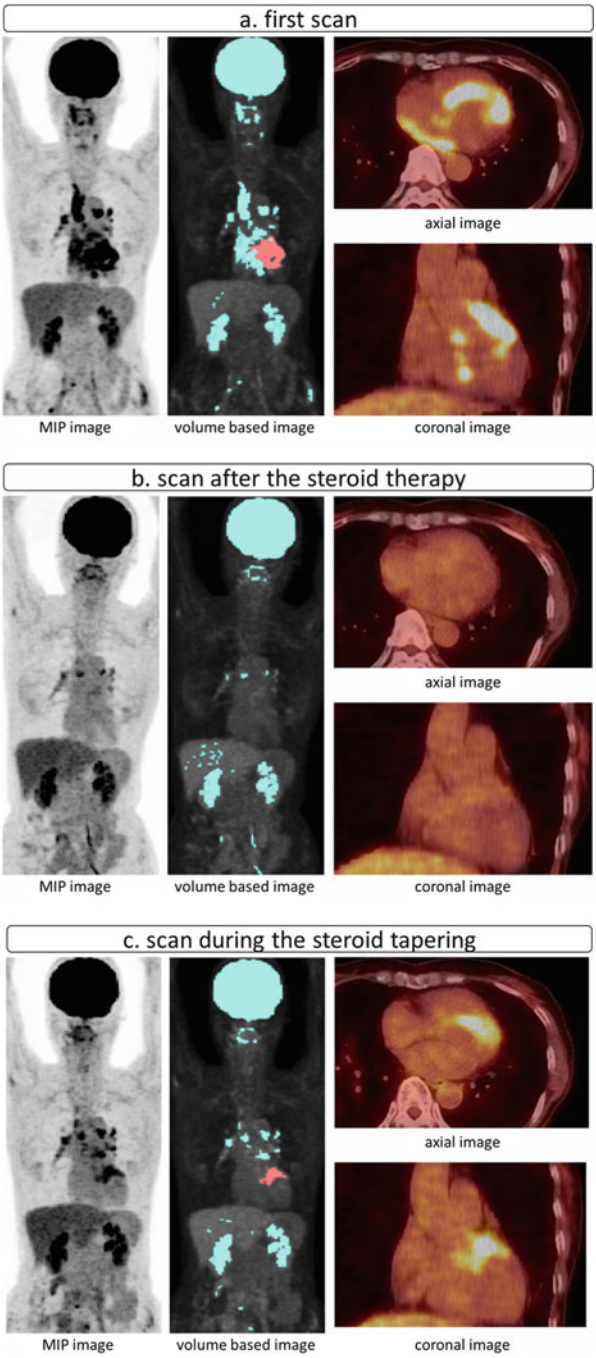

Fig. 16.4 Representative case.
This is a case of a cardiac sarcoidosis patient with uveitis and respiratory discomfort. She had a right bundle branch block and right axis deviation on the electrocardiograph and thinning of the

in a number of fields of cardiac and inflammation diseases like it is for malignant tumors (Fig. 16.4).

16.8 Conclusions

Observations from ^{18}F-FDG PET images are a useful diagnostic tool to detect active inflammatory lesions associated with cardiac sarcoidosis. For a precise evaluation of the extent and severity of cardiac involvement, long fasting and dietary modifications, such as observing a low-carbohydrate or a high-fat diet, are recommended approaches to reduce physiological myocardial ^{18}F-FDG uptake. The FFA level before the PET data acquisition could be a predictor for success in the suppression of physiological ^{18}F-FDG accumulation. Such ^{18}F-FDG PET images also enable therapy monitoring or risk stratification based on the quantitative accumulation determination. The quantification of the volume and intensity of ^{18}F-FDG uptake may also help predict the clinical outcomes and evaluate the efficiency of steroid treatment.

Conflicts of Interest None

Acknowledgments This study was supported in part by grants from the Innovation Program of the Japan Science and Technology Agency and a Hokkaido Heart Association Grant for Research.

Fig. 16.4 (continued) septal wall with severe hypokinesis on the echocardiograph. There was a clearly abnormal ^{18}F-FDG uptake in the LV wall as well as in the lymph nodes which indicated active inflammatory changes associated with sarcoidosis (**a**). The estimated maximum standardized uptake value (SUVmax) was 10.6, and the volume of the uptake was 76.1 ml (the threshold was obtained from the liver uptake) at the cardiac lesion. The ^{18}F-FDG PET [revealed the dramatic] showed a nearly total disappearance of the abnormal cardiac uptake after 4 weeks of therapy with prednisolone (**b**). However, the ^{18}F-FDG PET during the tapering of the prednisolone showed renewed ^{18}F-FDG uptake. Here, the estimated maximum standardized uptake value (SUVmax) was 6.2, and the volume of the uptake was 7.83 ml (the threshold was obtained from the liver uptake). This case indicates that ^{18}F-FDG was useful to evaluate the sarcoidosis activity and indicated the improvement during the therapy as well as the recurrence of the active sarcoidosis

References

1. Hunninghake GW, Costabel U, Ando M, et al. ATS/ERS/WASOG statement on sarcoidosis. American Thoracic Society/European Respiratory Society/World Association of Sarcoidosis and other Granulomatous Disorders. Sarcoidosis Vasc Diffuse Lung Dis. 1999;16:149–73.
2. Iannuzzi MC, Rybicki BA, Teirstein AS. Sarcoidosis. N Engl J Med. 2007;357:2153–65.
3. Sekhri V, Sanal S, Delorenzo LJ, Aronow WS, Maguire GP. Cardiac sarcoidosis: a comprehensive review. Arch Med Sci. 2011;7:546–54.
4. Baughman RP, Teirstein AS, Judson MA, et al. Clinical characteristics of patients in a case control study of sarcoidosis. Am J Respir Crit Care Med. 2001;164:1885–9.
5. Silverman KJ, Hutchins GM, Bulkley BH. Cardiac sarcoid: a clinicopathologic study of 84 unselected patients with systemic sarcoidosis. Circulation. 1978;58:1204–11.
6. Iwai K, Sekiguti M, Hosoda Y, et al. Racial difference in cardiac sarcoidosis incidence observed at autopsy. Sarcoidosis. 1994;11:26–31.
7. Ishida Y, Yoshinaga K, Miyagawa M, et al. Recommendations for (18)F-fluorodeoxyglucose positron emission tomography imaging for cardiac sarcoidosis: Japanese Society of Nuclear Cardiology recommendations. Ann Nucl Med. 2014;28:393–403.
8. Birnie DH, Sauer WH, Bogun F, et al. HRS expert consensus statement on the diagnosis and management of arrhythmias associated with cardiac sarcoidosis. Heart Rhythm. 2014;11:1305–23.
9. Manabe O, Yoshinaga K, Ohira H, et al. The effects of 18-h fasting with low-carbohydrate diet preparation on suppressed physiological myocardial (18)F-fluorodeoxyglucose (FDG) uptake and possible minimal effects of unfractionated heparin use in patients with suspected cardiac involvement sarcoidosis. J Nucl Cardiol. 2015. Aug. [Epub ahead of print]
10. Ohira H, Tsujino I, Yoshinaga K. (1)(8)F-Fluoro-2-deoxyglucose positron emission tomography in cardiac sarcoidosis. Eur J Nucl Med Mol Imaging. 2011;38:1773–83.
11. Manabe O, Ohira H, Yoshinaga K, et al. Elevated (18)F-fluorodeoxyglucose uptake in the interventricular septum is associated with atrioventricular block in patients with suspected cardiac involvement sarcoidosis. Eur J Nucl Med Mol Imaging. 2013;40:1558–66.
12. Manabe O, Yoshinaga K, Ohira H, et al. Right ventricular (18)F-FDG uptake is an important indicator for cardiac involvement in patients with suspected cardiac sarcoidosis. Ann Nucl Med. 2014;28:656–63.
13. Koiwa H, Tsujino I, Ohira H, Yoshinaga K, Otsuka N, Nishimura M. Images in cardiovascular medicine: Imaging of cardiac sarcoid lesions using fasting cardiac 18F-fluorodeoxyglucose positron emission tomography: an autopsy case. Circulation. 2010;122:535–6.
14. Manabe O, Oyama-Manabe N, Ohira H, Tsutsui H, Tamaki N. Multimodality evaluation of cardiac sarcoidosis. J Nucl Cardiol. 2012;19:621–4.
15. Hirata K, Kobayashi K, Wong KP, et al. A semi-automated technique determining the liver standardized uptake value reference for tumor delineation in FDG PET-CT. PLoS One. 2014;9, e105682.
16. Ahmadian A, Brogan A, Berman J, et al. Quantitative interpretation of FDG PET/CT with myocardial perfusion imaging increases diagnostic information in the evaluation of cardiac sarcoidosis. J Nucl Cardiol. 2014;21:925–39.